3

Modulation and Detection

As we discussed in Chapter 1, a digital modulator is simply a device for converting a discrete-time sequence of symbols from a finite alphabet, whether precoded or not, into continuous-time signals suitable for transmission by the physical channel provided. Likewise, a demodulator is a device for processing a noisy, perhaps distorted, version of the transmitted signal and producing numerical outputs, one per modulator symbol. This series of actions involves both deterministic and stochastic effects.

There are clearly many possible types of modulation processes, differing in the manner they manipulate an electromagnetic signal. Such manipulations include changing the amplitude, frequency, or phase angle of a sinusoidal signal, the polarization of the electromagnetic radiation, or the pulse position within a modulation interval. Some examples will follow in the next section. Some descriptions of modulation imply that modulation is only a conversion from a low-frequency (baseband) waveform to a high-frequency (carrier) signal, but we shall adopt a more unified view, that of a signal generator driven by a discrete-time, discrete-alphabet sequence.

Most classical modulation schemes are memoryless; that is, the *contribution* to the transmitted waveform induced by a given modulation symbol is defined purely by that symbol, and not the previous symbols. (This does not imply that the contribution a given symbol makes is limited to the time interval between successive symbols, as described later.) There are other important schemes, with "modulation" in their adopted name, that have memory. Normally, these are oriented toward spectrum control by introducing

constraints on the signal over several intervals. One example is *partial-response modulation*, in which the transmitted pulse amplitude depends on several previous information bits. In *continuous-phase modulation*, the phase angle of the transmitted carrier is forced to be continuous at all points in time and often to have continuous derivatives, again to effect a compact power spectrum. Here again, the signaling process has memory.

In this book, however, we will **interpret modulation to be a memoryless process.** Any constraints put into the signal, as just described, will be lumped into the device we will call the channel encoder, whose traditional attribute is a good deal of memory in its input/output relation. Such a definition is perhaps controversial, for it does not always provide the most straightforward description of a signaling process. However, it provides a convenient decomposition that still offers a unified view of coding and modulation. Furthermore, this decomposition can illuminate the total signal design problem and even lead to better designs than obtainable without this perspective. We will return to this later. This decomposition should not be construed to mean that we should always separate the functions of modulation and coding; in fact, they must be seen as a tandem in general for best performance. Our view merely is to separate the signaling process into a stage with memory and one without. Finally, if the signaling process is memoryless, and the cascade of modulator, channel, and demodulator produces zero intersymbol interference (ISI), then an optimal decision regarding the message can be made in symbol-by-symbol fashion.

Before proceeding with a thorough study of modulation and detection theory, we introduce a generic channel model to be used in the remainder of the book, which in its various special cases encompasses most of the practically important waveform channel effects.

3.1 A TRANSMISSION MODEL

A quite general model for a single-sender, single-receiver digital communication system is depicted in Figure 3.1.1. This model incorporates the most interesting problems faced by the designer of digital communication systems, including channel distortion due to filtering, attenuation, amplitude fading effects, and, of course, additive noise. Before delving into a description of the channel effects, we will consider more specifically some notation about modulators.

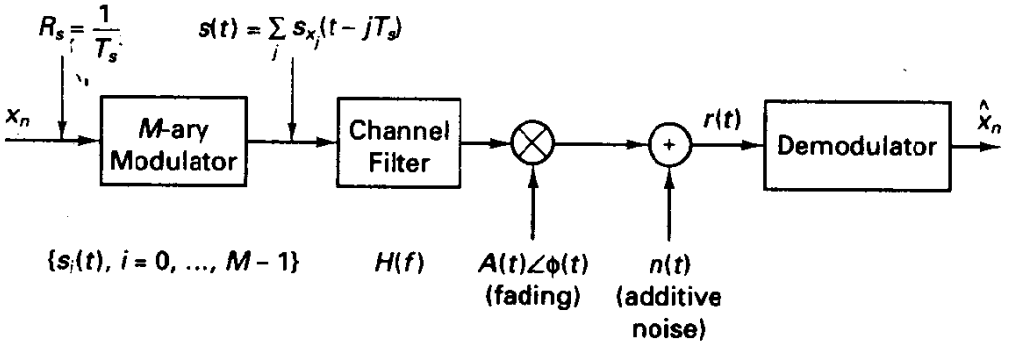

Figure 3.1.1 Generic system model for modulation and demodulation.

3.1.1 Digital Modulation

Every T_s seconds, in response to an input x_n from an alphabet of size M, the modulator produces a signal $s_{x_n}(t)$ from among a set of M real waveforms, $\{s_i(t), i = 0, 1, \ldots, M-1\}$. We refer to this process as ***M-ary modulation***. The waveforms may represent voltages, currents, electric field intensity, and so on.

Often, the M signals are confined to a time interval of length T_s, but this is not a necessary requirement, and in some cases, pulse overlap is useful for spectrum management purposes. In any case, $R_s = 1/T_s$ is the ***signaling rate*** in symbols per second. Usually, M is a power of 2, that is, $M = 2^m$, so we can think of each symbol as attempting to convey m bits per symbol, and the ***bit rate*** then would be $R_b = m/T_s = mR_s$ bits/second, or bps.[1]

The aggregate signal $s(t)$ produced by the modulation and coding system is a superposition, in time, of selections from the modulator set

$$s(t) = \sum_n s_{x_n}(t - nT_s), \tag{3.1.1}$$

where $\{x_n\}$ is the M-ary sequence of modulator inputs. Such a representation is possible because of the assumption of memoryless action by the modulator. It will be convenient at times to think of (3.1.1) as representing a sample function from a random process; to make such a process wide-sense stationary, it is customary to embed in each sample function random parameters for such quantities as the beginning of the symbol interval and carrier phase angle.

We shall first assume that signals are amplitude normalized so that *at the transmitter* the expected energy expended per symbol is E_s joules, where we define electrical energy relative to a 1-Ω impedance. Thus,

$$E_s \triangleq E\left[\int s_i^2(t)\,dt\right] = \frac{1}{M}\sum_{i=0}^{M-1}\int s_i^2(t)\,dt, \tag{3.1.2}$$

where the expectation is with respect to selection of the signal index, and we have assumed equiprobable signal selection. Integration in (3.1.2) is over the duration of the signals, whether of finite or infinite duration. Normally, we may equate the expected energy with the energy obtained by a time-averaging operation on a single sample function of the modulator output process. [Technically, the energy per symbol defined in (3.1.2) may not represent the actual average energy expended in the signal of (3.1.1) due to possible signal overlap in time; even in this case we usually find equality in practice, and we shall overlook this minor issue at this point.]

It is now useful to consider several practical modulation techniques to capture the essential ideas. These examples span a large range of desired transmission rates.

Pulse Amplitude Modulation with Four Levels

Suppose a 4-ary signal set is constructed as

$$s_i(t) = a_i h_T(t), \qquad i = 0, 1, 2, 3, \tag{3.1.3}$$

[1]The actual entropy per input symbol may be less if the modulator input is coded in redundant fashion or if the inputs are memoryless but not equiprobable.

where a_i is selected from the set $\{-3a, -a, a, 3a\}$ according to the message index to be sent, and $h_T(t)$ is a pulse shape common to all signals. The information is thus conveyed by the amplitude modulation of a basic signaling pulse; hence the terminology pulse amplitude modulation (PAM).

In this situation, the energy attached to the various signals differs. Integration of the squares of the various signals and averaging over message selection gives that the average energy expended is $5a^2E_p$, where $E_p = \int |h_T(t)|^2 dt$, so to attain a certain average energy E_s, we scale according to $a = (E_s/5E_p)^{1/2}$.

This 4-ary modulation technique forms the basis of the primary rate interface for ISDN.[2] There the signaling rate is $R_s = 80$ ksps, with an implied bit rate of $R_b = 160$ kbps.

4-ary Phase Shift Keying

Suppose we again adopt $M = 4$ but define the four signals to be bursts of sinusoidal signal having a center frequency ω_c and fixed phase angle selected from $\{0, \pi/2, \pi, 3\pi/2\}$ radians, dependent on the digital input signal. Thus,

$$s_i(t) = \left(\frac{2E_s}{T_s}\right)^{1/2} \cos\left(\omega_c t + i\frac{\pi}{2}\right), \quad i = 0, 1, 2, 3, \quad 0 \le t < T_s \tag{3.1.4}$$

Here, each signal has the same energy, $E_i = E_s$, assuming either $\omega_c T_s = n\pi$ or more realistically that $\omega_c T_s \gg 1$, and the average energy is then E_s as well.

This modulation format represents a typical choice in digital satellite communications, whereby choosing $R_s = 772$ kHz, we achieve a bit rate $R_b = 1.544$ megabits/second, the T1 rate in the North American digital transmission hierarchy. Such a channel could support teleconference quality video service, for example, or 24 simultaneous digitized voice conversations. Other transmission rates are, of course, possible with this modulation format.

Binary Frequency Shift Keying

With $M = 2$, we implement a frequency modulation scheme that selects the one of two sinusoidal oscillators having frequencies f_0 and f_1. The oscillator phase angles are θ_0 and θ_1. The amplitude is again chosen so that E_s is in fact the average energy per symbol interval. Thus,

$$s_i(t) = \left(\frac{2E_s}{T_s}\right)^{1/2} \cos(2\pi f_i t + \theta_i), \qquad i = 0, 1, \quad 0 \le t < T_s \tag{3.1.5}$$

This forms the essence of the transmission scheme for 300 bps modems (now rather hard to find!) for the public switched telephone network. There the two frequencies (in one of the bidirectional paths) are 1070 and 1270 Hz.

A variation on this method uses a single oscillator that is frequency modulated to one of two frequencies, but this is not strictly speaking a memoryless modulation process because the phase angle at the beginning of any interval depends on the entire past data symbols.

---

[2]Integrated Services Digital Network, an emerging international digital transmission network that seeks to integrate multimedia services of voice, data, video, and the like. A recent reference is J. W. Griffiths, *ISDN Explained*, Wiley, New York, 1990.

3.1.2 Channel Filtering

The transmitted signal $s(t)$ may first be acted on by a linear filter, described by a frequency response function $H(f)$ or by its impulse response, $h(t)$, which forms a Fourier transform pair. Such filtering action represents a fact of life for the communication engineer. Bandwidth limitations of the channel, whether due to the physics of the channel itself or electronic equipment used in the communication process (possibly imposed by regulatory constraints), affect the signals we transmit. In some situations, the effect on the signal is negligible, if the available bandwidth is much larger than the intended signaling rate. When this is not the case, intelligent design can perhaps mitigate the impact. In still other situations, channel dispersion due to such filtering is the dominant limitation on data integrity.

Examples of this band limitation occurring in practice are found in the public switched telephone network (PSTN), engineered in the days when only analog voice transmission was of interest, and in a typical satellite transponder. Typical frequency responses for each are shown in Figures 3.1.2a and 3.1.2b. Note that both amplitude-versus-frequency and phase-versus-frequency descriptions are required.[3]

The limited frequency response of the voice-band channel is the result of several factors. At the high-frequency end, distributed inductance and capacitance of the twisted-wire pair connecting customer premises to central offices induce significant attenuation for frequencies above 3 kHz. On the other hand, transformer-coupling implies poor low-frequency response (below about 200 Hz). For speech transmission, the effect is quite innocuous; after all, the transmission channel was designed for acceptable speech transmission, but for high-speed data communication over the voice-band channel, the effect of this limited frequency response proves to be a severe impairment. This kind of channel would be referred to in the literature as a ***baseband*** channel, meaning that the available frequency response extends from (essentially) zero frequency to some upper limit, usually a soft constraint, as in Figure 3.1.2a.

The satellite channel on the other hand (whose frequency response is specified in Figure 3.1.2b) would be classified as a ***bandpass*** channel, simply meaning that the bandwidth available is a small fraction of the center frequency. Typically, a satellite transponder may provide a 30-MHz usable range of frequencies situated in the microwave region, say near 4 GHz. It is not essential to make a strong distinction between these two categories, and appropriate signal analysis tools can accommodate both cases together. However, the separation is rather common in the literature, where we often find a distinction between baseband signaling and carrier modulation, respectively.

It might be suggested that we incorporate the effect of the channel filter into the description of the signal set, defining the transmitted signals as those that emerge from the filter $H(f)$. We do not for several reasons. First, the signaling process could no longer be described in memoryless fashion. Second, we will be interested in the effect of various channel filters on certain standard signal sets and, in particular, to evaluate performance against the no-filtering case. Finally, the point at which a power constraint

[3]Phase information is usually conveyed through the frequency derivative of phase, called the group delay function.

ATT Requirements for Two-point or Multipoint Channel Attenuation Distortion

	Frequency Band (Hz)	Attenuation[a] (dB)
Basic requirements	500 – 2500	–2 to +8
	300 – 3000	–3 to +12
C1 conditioning	1000 – 2400	–1 to +3
	300 – 2700	–2 to +6
	2700 – 3000	–3 to +12
C2 conditioning	500 – 2800	–1 to +3
	300 – 3000	–2 to +6
C4 conditioning	500 – 3000	–2 to +3
	300 – 3200	–2 to +6
C5 conditioning	500 – 2800	–0.5 to +1.5
	300 – 3000	–3 to +3

ATT Requirements for Two-point or Multipoint Channel Envelope Delay Distortion

	Frequency Band (Hz)	EDD (μs)[a]
C1 conditioning	800 – 2600	1750
	1000 – 2400	1000
C2 conditioning	1000 – 2600	500
	600 – 2600	1500
	500 – 2800	3000
C4 conditioning	1000 – 2600	300
	800 – 2800	500
	600 – 3000	1500
	500 – 3000	3000
C5 conditioning	1000 – 2600	100
	600 – 2600	300
	500 – 2800	600

[a]Maximum inband envelope delay difference.

Figure 3.1.2a Specified amplitude and delay distortion limits for voiceband data links. (*Source: Telecommunication Transmission Engineering*, Vol. 2, 2nd ed. American Telephone & Telegraph Co., New York.)

on transmission is usually enforced is ahead of the channel filtering,[4] and it is important to be able to explicitly identify the transmitted signal in the mathematical model.

For most of the text, we shall assume that the channel filter is nondistorting; that is, it has constant gain and linear phase versus frequency over the frequency range occupied

[4]In fact, the significant channel filtering may be much nearer the demodulator.

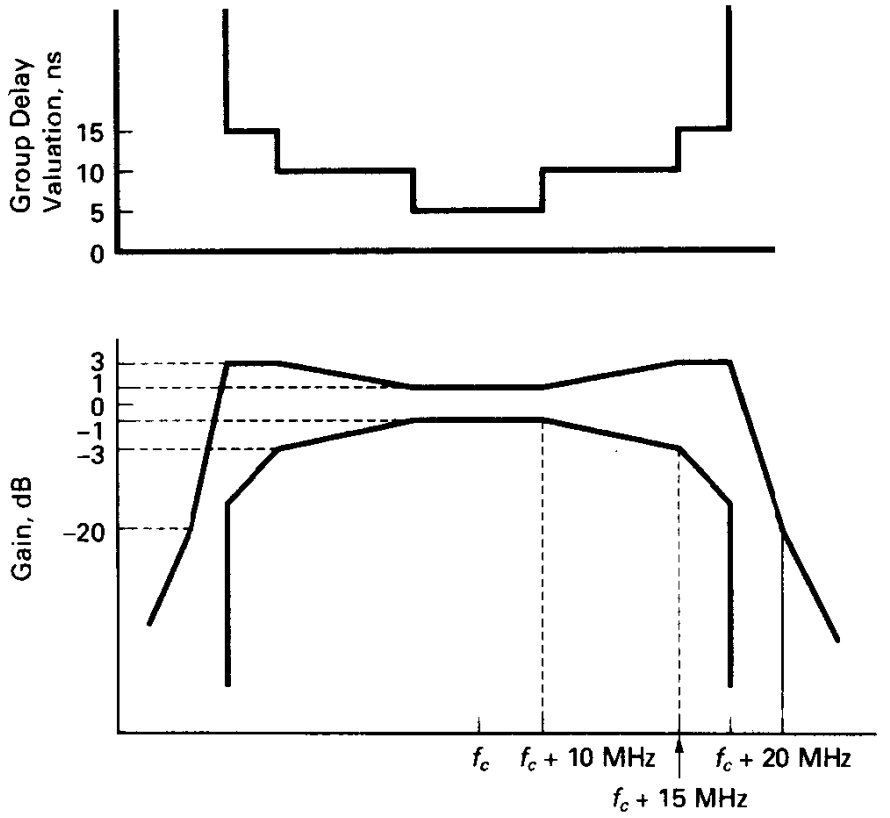

Figure 3.1.2b Typical envelope for amplitude and delay distortion, satellite transponder with nominal 36-MHz bandwidth.

by the signal set (see [1] or Exercise 3.1.1). We include the presence of channel filtering at the outset only for completeness of description. It is convenient to adopt a gain of unity for the filter so that the average energy per symbol at the filter output is still E_s joules. If the gain is not 1, this scaling can be subsumed into the definition of channel gain. Similarly, we will commonly adopt a zero-delay assumption for the channel, but this should not hide the need to establish proper timing in the demodulator.

3.1.3 Channel Gain and Fading

The next component of the model accounts for the bulk channel gain and the channel phase/frequency shift (if carrier transmission is involved). We can incorporate both effects using complex envelope notation for the signal. Complex signal notation simply regards the actual bandpass signal $s(t)$ as

$$s(t) = \mathrm{Re}\left(\tilde{s}(t)e^{j\omega_c t}\right), \tag{3.1.6}$$

where $\tilde{s}(t)$ is defined implicitly as the ***complex envelope*** of the signal, relative to the adopted radian frequency of the carrier ω_c. It is possible to perform analysis strictly on the low-pass signal $\tilde{s}(t)$, with the high-frequency dependence completely suppressed

and reinserted at the end [1]. This is essentially the method behind phasor analysis of steady-state circuits excited by sinusoids.

We shall represent the channel gain in Figure 3.1.1 by the complex envelope process $A(t)e^{j\theta(t)}$, where $A(t)$ represents the amplitude scaling in the channel, and $\theta(t)$ represents the aggregate channel phase shift due to propagation delays and oscillator frequency offsets. [Notice that signal frequency change due to Doppler shift or oscillator frequency offsets can be subsumed into $\theta(t)$ by a linear time dependence; that is, $\theta(t) = \Delta\omega t$.] Our representation of the channel gain process means then that if the transmitted signal is a unit-amplitude, unmodulated sinusoid, $\cos(\omega_c t)$, then $\tilde{s}(t) = 1$ from (3.1.6) and the received signal is

$$\begin{aligned} r(t) &= \mathrm{Re}\,(\tilde{s}(t)A(t)e^{j\theta(t)}e^{j\omega_c t}) \\ &= A(t)\cos[\omega_c t + \theta(t)], \end{aligned} \tag{3.1.7}$$

showing amplitude and phase modulation by the time-varying channel.

In many cases, $A(t)$ is regarded as constant, and if chosen as unity, then the average energy per symbol *at the demodulator* (the important location to specify this value) is also E_s. Of course, few channels have unit gain from transmitter to receiver, but this scaling issue will always be avoided by speaking of the received signal energy level relative to the noise level in performance analysis. Communication link analysis ultimately supplies this number, whether we are dealing with a cable medium, a microwave line-of-sight link, or an optical fiber channel. E_s is related to average received power, P_r, through $E_s = P_r T_s$.

In other important cases, the channel gain is modeled as time varying, primarily due to conditions loosely referred to as "fading" (see [2] for a survey of such channels). Such fading conditions are also physical in their origin. In mobile radio systems operating at frequencies of several hundred megahertz, fading occurs due to time-varying recombination of electric field wavelets having differing time delay after reflection from buildings, hills, trucks, and the like [3]. In VHF over-the-horizon digital communication using tropospheric scattering, fading is experienced at the receiver due to time-varying multipath propagation through the lower layers of the atmosphere. Finally, some satellite links may experience time varying signal levels due to ionospheric scintillation (below 1 GHz) or due to atmospheric absorption (increasingly significant above 10 GHz).

In our treatment of fading we will assume that the time variations of $A(t)$ are ***slow*** compared to the symbol rate R_s, so over a given signaling interval, the amplitude scaling factor may be treated as constant. More precisely, we model $A(t)$ as a stationary random process whose autocorrelation function is such that $R_A(\tau) \approx R_A(0) \equiv 1$ for $\tau \leq T_s$. Figure 3.1.3 depicts a typical sample function of such a slow-fading process $A(t)$. In practice, this slow-fading assumption seems routinely justified, given the demand for high signaling rates and the relatively slow dynamics of fading processes, such as multipath in mobile radio, or atmospheric fading conditions. The implication is that in our analysis we can treat the channel as frozen over a single symbol or, in fact, several consecutive symbols, but still allow a long-term variation.

Also implicit in our fading model is an assumption of ***flat-fading***; that is, the gain is the same for all components of the signal spectrum. Transmission engineers speak of this as ***nonfrequency-selective fading***, in distinction to cases where the fading

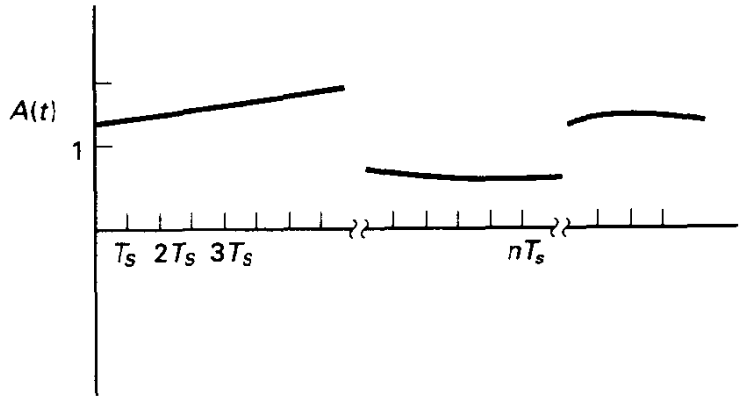

Figure 3.1.3 Sample function of fading process, amplitude $A(t)$ shown.

medium induces a certain time-varying selectivity for frequency bands, similar to the fixed selectivity performed by a channel filter.

Several models for the randomly varying amplitude $A(t)$ are prevalent in the literature, based on empirical or analytical study of physical channels. The ***Rayleigh fading*** model will be emphasized in our treatment, however, for several reasons. First, it is a rather worst-case situation for the design engineer. An increase in signal-to-noise ratio of several orders of magnitude over nonfading requirements is necessary for standard uncoded transmission formats to maintain a given error probability, as will be shown later in this chapter. Second, the Rayleigh model provides analytical convenience, which, like it or not, is a compelling justification. If we understand the principles here, it is straightforward to extend them to other appropriate fading models.

The Rayleigh model arises from the combination at the receiver of many randomly phased *point scatterer* contributions, each having a small fraction of the total received power. To see how this model is physically justified, consider the propagation setting shown in Figure 3.1.4, where the received signal is the sum of K scattered contributions. We assume that the gain of each scattered component is β and that each has a time-varying delay (due to motion of the medium or terminals) of $\tau_i(t)$. Suppose we let

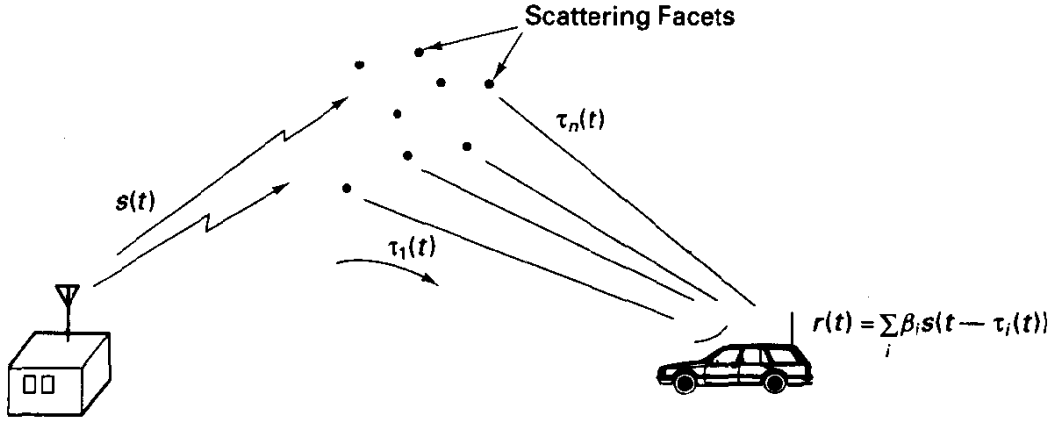

Figure 3.1.4 Idealized scattering model leading to Rayleigh fading.

the transmitted signal again be a *pure sinusoid*, $s(t) = \cos(\omega_c t)$. The received signal (without noise as yet) can be represented as

$$r(t) = \sum_{i=1}^{K} \beta \cos[\omega_c(t - \tau_i(t))]. \tag{3.1.8}$$

Using trigonometric expansion, this can be rewritten as

$$\begin{aligned} r(t) &= \beta \left[\sum_{i=1}^{K} \cos(\omega_c \tau_i(t)) \right] \cos(\omega_c t) \\ &\quad + \beta \left[\sum_{i=1}^{N} \sin(\omega_c \tau_i(t)) \right] \sin(\omega_c t) \\ &\triangleq \beta X(t) \cos(\omega_c t) - \beta Y(t) \sin(\omega_c t), \end{aligned} \tag{3.1.9}$$

where we have implicitly defined $X(t)$ and $Y(t)$. If we assume that the carrier frequency is large relative to the electromagnetic wavelength, and/or the spread of delays $\tau_i(t)$ is large, then $\omega_c \tau_i(t)$, at any time t, can be considered a uniform random variable on $[0, 2\pi)$. Furthermore, if the scatterers are moving (or, equivalently, if the terminals move relative to the scattering sources), the various terms contributing to $X(t)$ and $Y(t)$ can be modeled as independent random variables. By the central limit theorem developed in Chapter 2, we may approximate $X(t)$ and $Y(t)$ as Gaussian processes, assuming the number of scatterers K is large and that none dominates the others in strength. It is a routine matter to show further that $X(t)$ and $Y(t)$ are uncorrelated, and hence independent, due to their being Gaussian. Furthermore, (3.1.9) becomes in polar form

$$r(t) = \beta A(t) \cos[\omega_c t + \theta(t)] \tag{3.1.10}$$

with $A(t) = \left[X^2(t) + Y^2(t)\right]^{1/2}$, so we may argue as in Chapter 2 that the signal amplitude $A(t)$ is Rayleigh distributed at any time t.

The rate of change of $A(t)$ is clearly controlled by the rate of change of the relative delays of the scatterers. Rapidly changing scattering media, or rapidly moving terminals and fixed scatterers, produce fast fading, but again we suggest that the changes are typically slow relative to the time scale of typical signaling speeds. The model we described is somewhat idealized, but considerably more realistic situations produce essentially Rayleigh fading under the central limit theorem thesis.

These considerations lead to the model that the gain A during one symbol interval is a scalar Rayleigh random variable whose probability density function is given by

$$f_A(a) = 2ae^{-a^2}, \qquad a \geq 0. \tag{3.1.11}$$

The random variable is scaled so that the mean-square value of A is 1, and thus the *average*, or expected, received energy per symbol is still E_s.

Other physical assumptions lead to different fading models. For example, we might let one component of the aggregate in (3.1.8) be stronger than the rest, perhaps modeling a direct, unscattered propagation path. This leads to ***Rician fading***, whose distribution was described in Chapter 2. Still another common fading distribution is a ***log-normal*** model, for which the logarithm of the received signal strength is Gaussian distributed. This model derives from certain empirical observations.

Equation (3.1.10) shows that along with amplitude fading, the channel induces a random phase modulation of the signal, also slowly varying over a symbol duration, corresponding to a time-varying effective path length change. This phase angle θ is modeled as uniformly distributed on $[0, 2\pi)$. An important issue for system design is whether the receiver can determine the channel phase parameter and attempt what is known as ***coherent detection***. In fact, it is important to note that, even apart from fading effects, the carrier phase angle, measured at the receiver, is in general unknown due to unknown path lengths and oscillator phase shifts.

3.1.4 Noise Model

Finally, we come to the additive noise process, $n(t)$, in Figure 3.1.1. We regard it as a sample function from a stationary Gaussian process, $N(t)$, having zero mean and constant power spectral density, $N_0/2$ W/Hz (two-sided).[5] Furthermore, the noise process is independent of and additive to the signal. This is commonly referred to as ***additive white Gaussian noise*** *(AWGN)* and is the archetypal communication noise model for radio and optical frequency systems. Such a process cannot physically exist, as discussed in Chapter 2, because it presumes a signal with infinite bandwidth and infinite power, both of which violate notions about physical systems. Alternatively, the autocorrelation function, $R_n(\tau) = (N_0/2)\delta(\tau)$, indicates that the process has zero correlation time, which is equally strange to contemplate. Nonetheless, these difficulties can be easily finessed; any communication system we encounter will have finite bandwidth (for practical intents), and we simply model the noise process to have fixed power spectral density well beyond this region of interest. Although we will not dwell on the physics of such noise processes, their origins are principally as follows:

1. Thermal noise in electrical circuits
2. Shot noise processes developed in electronic or photonic devices
3. Electromagnetic radiation from the earth, sun, and other cosmic sources of radiation

Interested readers are referred to Van der Ziel's book [4], a classic on noise phenomena and modeling.

Although we shall usually assume that the receiver noise level is fixed, it is straightforward to allow the noise level to vary, perhaps on and off in some probabilistic fashion, to represent hostile interference or jamming.

3.1.5 Model Limitations

Before proceeding, it should be recognized that all cases of possible interest are not accommodated by our channel model. First, it is a ***linear*** model, and some important channels in practice are nonlinear, typically due to nonlinear amplifiers. Satellite transponders exhibit such nonlinearities, as do other high-power transmitters.

[5]This implies that the noise power measured in a conceptual 1-Hz band of spectrum is N_0 watts.

Another limitation is that, although we have allowed the channel to be time dispersive [in the form of nonideal $H(f)$], we have assumed this characteristic to be time invariant. (The time-varying channel gain is not frequency selective by assumption.) A more general model might have allowed a time-varying transfer function of the form $H(f, t)$. This is an important phenomenon for long-haul HF radio communications by ionospheric wave guiding and line-of-sight digital microwave radio [5].

Also, the adopted model is effectively nonfrequency dispersive, meaning that the channel gain/phase modulation of the signal is so slow that appreciable change does not occur over T_s seconds. (This is in actuality the slow-fading assumption made earlier.) The name derives from the fact that such a channel will not produce spectral broadening, or dispersion, of the transmitted signal. Once again, the claim is that this is generally the case for typical high-speed digital communication. Both of these extensions of the model are simply beyond the intended scope of this presentation. Topics studied in this text are, however, the basis for treating these more sophisticated models.

The noise model does not account for non-Gaussian noise, which may be present due to interference from other signals, electrostatic discharges in the atmosphere, or electrical machinery. Modeling of such processes is generally ad hoc, receiver optimization tends to be somewhat heuristic, and performance analysis is "special case" in nature. Also, nonwhite noise is excluded at the outset; it is usually the case that the additive noise processes have power spectra that are nearly constant over the range of frequencies larger than that occupied by the signal. Again, the AWGN model provides a framework for further study.

Finally, the channel does not apparently incorporate such simple communication channel models as the binary symmetric channel (BSC), seen in virtually every text on coding techniques and introduced in Chapter 2. However, this and other discrete channels are derivatives of the model found in Figure 3.1.1 simply by discretizing, or quantizing, the outputs of the demodulator. In fact, this is always how discrete channel models emerge. For example, a binary symmetric channel can be derived by sign-detecting the output of a Gaussian noise channel with bipolar signaling. In light of the data-processing theorem of Chapter 2, such quantization is usually information destroying and generally unadvisable in coded systems. We shall make this more precise in subsequent chapters.

3.2 SIGNAL SPACES

As a prelude to the study of optimal demodulation and receiver implementation, we now represent an M-ary signal set by an orthonormal series expansion, quite analogous to the classical Fourier series representation. By using the expansion coefficients as coordinates in a space defined by the expansion basis functions, we capture a powerful geometric interpretation of demodulation theory and indeed the general signal design problem. This tool will also supply the bridge between decision theory for sequences of random variables and waveform problems. This viewpoint was popularized by Wozencraft and Jacobs [6]. Texts on signal theory by Franks [7] and Weber [8] are also fine references.

3.2.1 Orthonormal Basis Sets

Consider a set of real waveforms $\{\phi_m(t), m = 0, 1, \ldots\}$ defined over some common interval (T_i, T_f). The set may or may not be finite, and the time interval likewise: The set of functions is said to be ***orthonormal*** if

$$\int_{T_i}^{T_f} \phi_i(t)\phi_j(t)\, dt = \delta_{ij} = \begin{cases} 1, & i = j, \\ 0, & i \neq j. \end{cases} \tag{3.2.1}$$

We may say that the functions $\phi_j(t)$ are unit energy, since if $\phi_j(t)$ were a voltage impressed across a 1-Ω resistance, the integral-square value of the function (which is its energy) is 1.

It is easy to construct very large orthonormal sets. A familiar example to engineers is the Fourier set for finite intervals $T = T_f - T_i$, the infinite set of sinusoids whose frequencies are integer multiples of $1/T$:

$$\{\phi_m(t)\} = \left\{ \left(\frac{1}{T}\right)^{1/2}, \left(\frac{2}{T}\right)^{1/2} \cos m\omega_0 t, \left(\frac{2}{T}\right)^{1/2} \sin m\omega_0 t, \ldots \right\}, \qquad m = 1, 2, \ldots, \tag{3.2.2}$$

where $\omega_0 = 2\pi/T$. Simple calculations show that (3.2.1) holds for any pair of this infinite set.

Another example is a finite set of N nonoverlapping pulses:

$$\phi_m(t) = \left(\frac{1}{T'}\right)^{1/2} \text{rect}\left[\frac{t - mT'}{T}\right], \qquad m = 0, 1, 2, \ldots, N - 1, \tag{3.2.3}$$

with $T = (T_f - T_i)/N$, and rect$[t/T]$ denoting a pulse of unit height beginning at $t = 0$ and lasting T seconds. Members of these two orthonormal sets are shown in Figure 3.2.1.

Given a class of deterministic signals $\{s_i(t), i = 1, 2, \ldots\}$, each having finite energy, suppose we form an N-term series expansion of the ith signal in terms of an orthonormal set of functions:

$$s_i^{(N)}(t) = \sum_{m=0}^{N-1} s_{im}\phi_m(t). \tag{3.2.4}$$

The expansion coefficients, s_{ik}, are found by

$$s_{ik} = \int_{T_i}^{T_f} s_i(t)\phi_k(t)\, dt, \tag{3.2.5}$$

which follows from multiplying both sides of (3.2.4) by $\phi_k(t)$ and integrating over (T_i, T_f). Equation (3.2.5) can be interpreted as the projection of the ith signal onto the kth basis function, and the expansion in (3.2.4) represents the orthogonal projection of $s_i(t)$ onto the space spanned by the N basis functions. One motivation for using orthonormal basis functions is that the coefficients can be found separately in any order, and more terms in an expansion are therefore easily added if necessary. Furthermore, orthonormality induces important geometric properties related to the set of signals.

For a general class of signals, an N-term representation may never be perfect for finite N, but if the set $\{\phi_m(t)\}$ is ***complete*** for the class of signals, then the energy in the

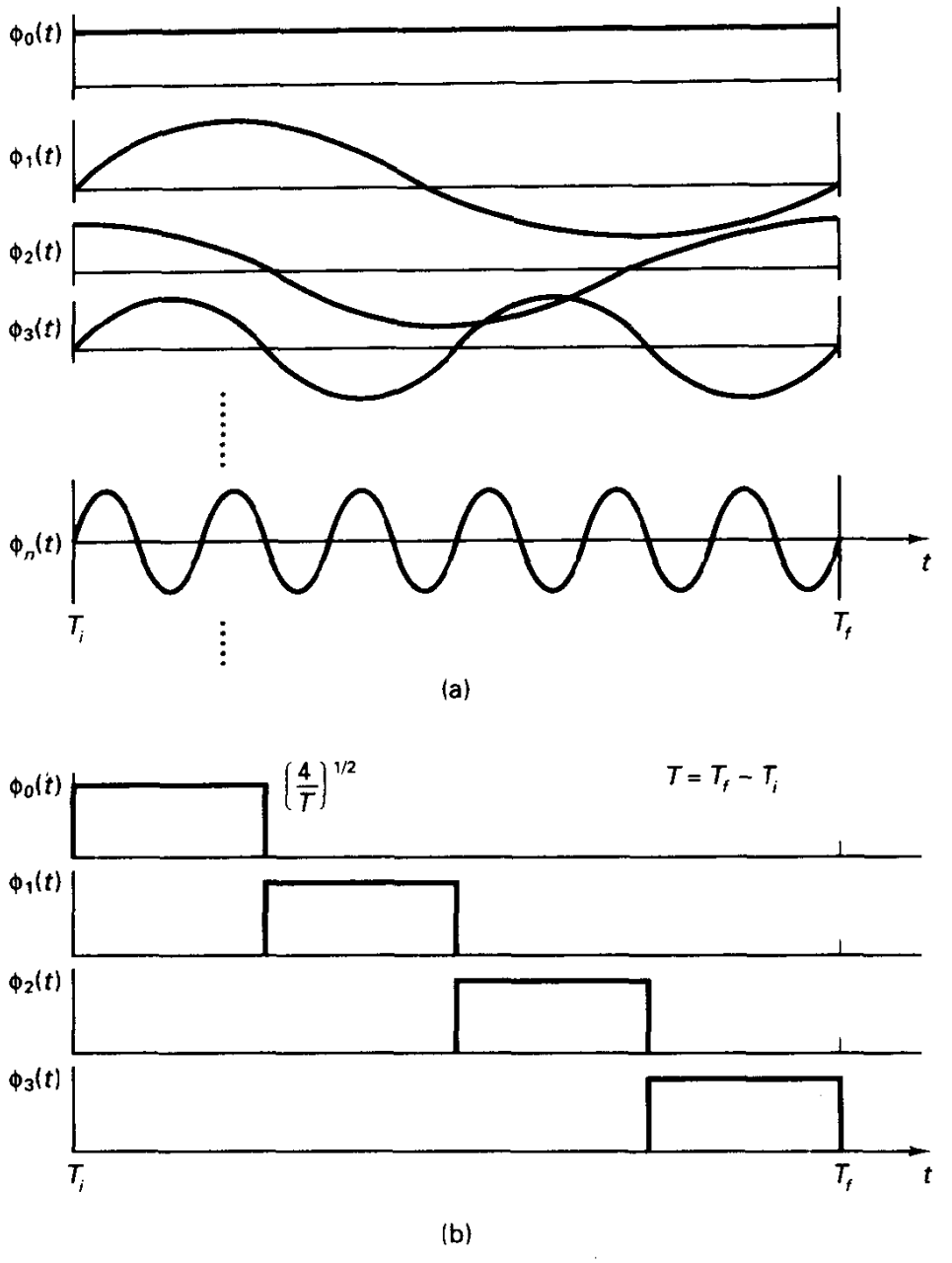

Figure 3.2.1 Example of simple orthonormal bases. (a) Fourier orthonormal set; (b) nonoverlapping basis set, $N = 4$.

error signal can be made arbitrarily small as N grows; that is,

$$\lim_{N\to\infty} \int \left[s_i(t) - s_i^{(N)}(t)\right]^2 dt = 0. \tag{3.2.6}$$

We frequently term such a set $\{\phi_m(t)\}$ a ***complete orthonormal basis*** for a given class of signals. For example, the Fourier set is known to be a complete orthonormal basis for the class of signals having duration T seconds, with finite energy, a finite number of

maxima/minima, and finitely many discontinuities (the Dirichlet conditions). At points of discontinuity, convergence is to the midpoint of the discontinuity, but the integral-square error (3.2.6) diminishes to zero for all signals in the class as more expansion terms are added.

3.2.2 *M*-ary Signal Constellations

We are now ready to describe the actual M-ary set of modulator waveforms using orthonormal series expansions. We can always provide *exact* expansions with *finite* basis sets having $N \leq M$ elements, and minimal sets will be provided by the Gram–Schmidt orthogonalization procedure [9]. (Haphazard selection of basis functions may not yield finite basis sets; for example, the Fourier set does not provide an exact finite series representation for even a single rectangular pulse signal.)

Before describing the Gram–Schmidt procedure, we should visualize what the expansion provides. First, every signal $s_i(t)$ is mapped to a point in N-dimensional Euclidean space called ***signal space***, each point represented as $\mathbf{s}_i = (s_{i0}, s_{i1}, \ldots, s_{i(N-1)})$, where N is the size of the basis set. Either setting forms a complete description of a signal set, once the basis set is specified. Figure 3.2.2 illustrates the decomposition and reconstruction of signal waveforms in terms of its signal space coordinates.

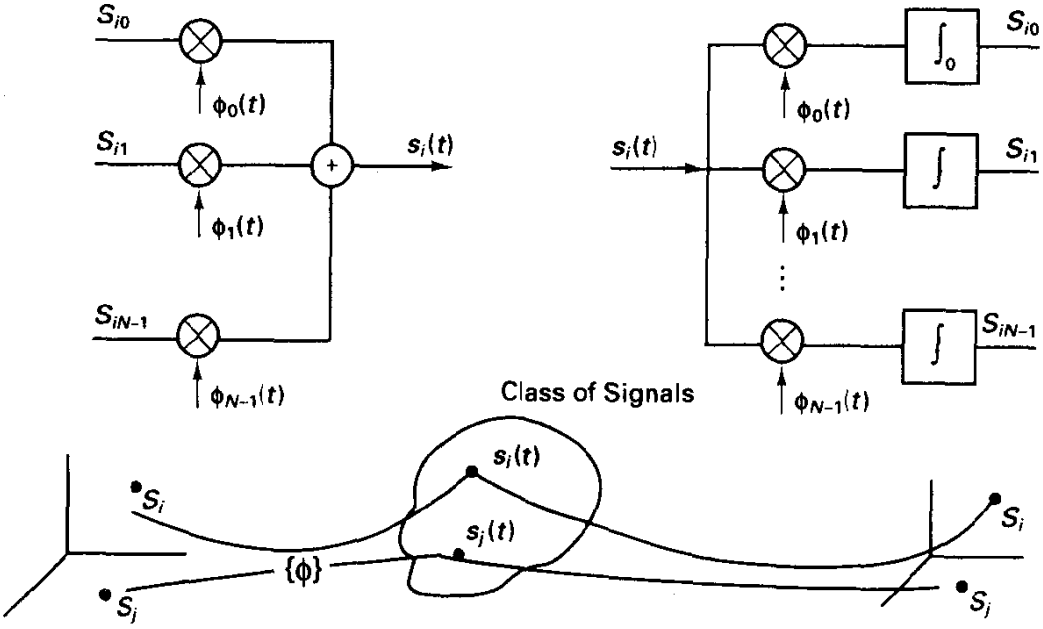

Figure 3.2.2 Signal generation and coefficient recovery.

The collection of M points in N-space is called the ***signal constellation***, and it provides a geometry for studying modulation and coding techniques. For example, the squared distance from the origin to any point in signal space can be easily shown to equal the energy in the corresponding signal, and the L_2-distance between waveforms (the integral of the squared difference signal) is precisely the same as the squared distance

computed between points in Euclidean signal space.[6] To verify the former claim, we expand $s_i(t)$, square, and integrate:

$$E_i = \int_{T_i}^{T_f} s_i^2(t)\,dt = \int_{T_i}^{T_f} \sum_{m=0}^{N-1}\sum_{k=0}^{N-1} s_{im}\phi_m(t)s_{ik}\phi_k(t)\,dt$$

$$= \sum_m \sum_k s_{im}s_{ik}\int_{T_i}^{T_f} \phi_m(t)\phi_k(t)\,dt = \sum_m \sum_k s_{im}s_{ik}\delta_{mk} \qquad (3.2.7)$$

$$= \sum_{m=0}^{N-1} s_{im}^2.$$

The second property is shown by expressing the squared intrasignal distance as

$$d_{ij}^2 = \int_{T_i}^{T_f} \left[s_i(t) - s_j(t)\right]^2 dt$$

$$= \int \left[\sum_m s_{im}\phi_m(t) - \sum_n s_{in}\phi_n(t)\right]^2 dt. \qquad (3.2.8)$$

Upon expanding the right-hand side and using the orthonormality property of the basis functions, we have

$$d_{ij}^2 = \sum_m (s_{im} - s_{jm})^2. \qquad (3.2.9)$$

Another benefit this representation affords is an immediate assessment of the ***dimensionality*** of the signal set, to which bandwidth occupancy is in some sense proportional, as we will see in Section 3.7. Finally, the number and form of the basis functions indicate in rough measure the complexity of the modulating and demodulating equipment.

As to the choice of basis functions, many sets $\{\phi_m(t)\}$ are possible. For purposes of minimizing complexity and correctly visualizing key properties of modulator signal sets, we should seek a set that is minimal, that is, N is as small as possible, and that is composed of simple functions. In many classical signaling formats, the proper choice is obvious by inspection. For example, suppose our modulator utilizes the binary signal set of Figure 3.2.3. An appropriate set of basis functions would be the scaled versions of the signals themselves, since the original two signals are already orthogonal. These basis functions are also shown in Figure 3.2.3, along with the two-dimensional signal-space representation. We reemphasize the distance claims made previously; each signal has squared distance from the origin of $E_s = A^2T_s/2$, which is the same as the energy in each waveform. Likewise, the squared distance between constellation points $\mathbf{s}_0$ and $\mathbf{s}_1$ is A^2T_s, which is just the same as the square of the L_2-distance between $s_0(t)$ and $s_1(t)$. We could alternatively employ four nonoverlapping rectangular pulses as a basis set, but this would not be minimal; also the Fourier set would provide a representation that converges asymptotically, but which is infinite dimensional.

A slightly less obvious basis construction pertains to M-ary PSK (phase shift keying) modulation, where the M signals are merely phase-shifted versions of a carrier

[6]The importance of L_2-distance will become apparent shortly in our detection theory study.

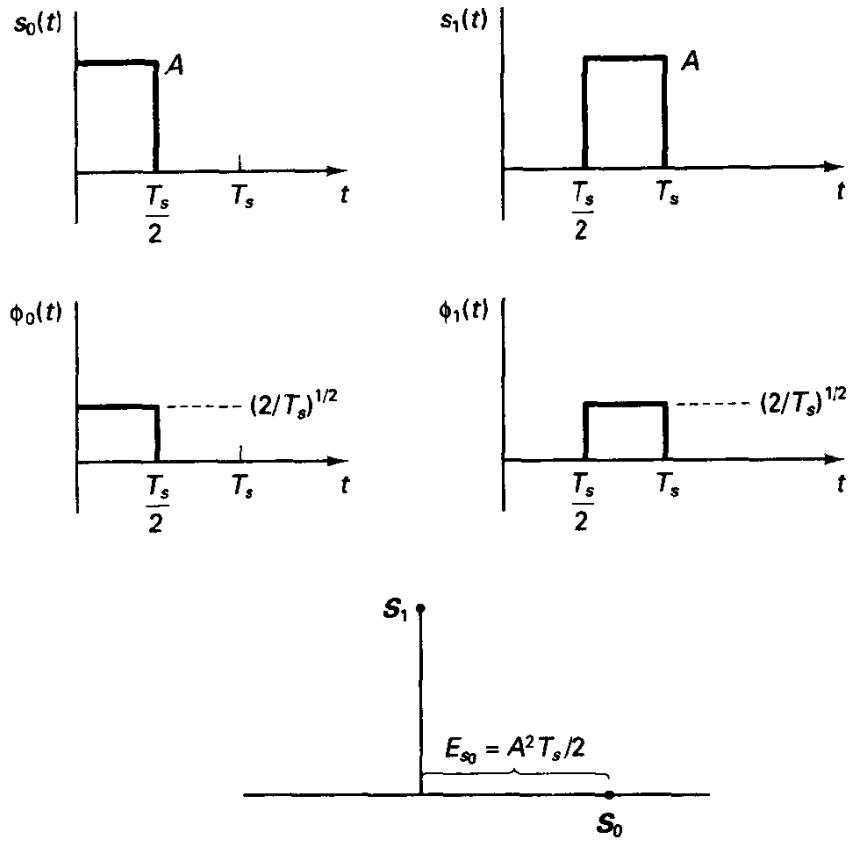

Figure 3.2.3 Two orthogonal signals and the obvious basis set.

sinusoid, lasting T_s seconds, with the phase shift being a multiple of $2\pi/M$ radians:

$$s_i(t) = \left(\frac{2E_s}{T_s}\right)^{1/2} \cos\left(\omega_c t + \frac{2\pi i}{M}\right), \qquad i = 0, 1, \ldots, M-1, \quad 0 \le t \le T_s. \tag{3.2.10}$$

By trigonometric identities it is obvious that any such signal is expressible in terms of two orthonormal functions[7]

$$\phi_0(t) = \left(\frac{2}{T_s}\right)^{1/2} \cos \omega_c t, \qquad \phi_1(t) = \left(\frac{2}{T_s}\right)^{1/2} \sin \omega_c t, \qquad 0 \le t \le T_s, \tag{3.2.11a}$$

so M-PSK signal sets have two-dimensional constellations (actually one-dimensional if $M = 2$). The signal-space coordinates of each signal are given by

$$s_{i0} = E_s^{1/2} \cos\left(\frac{2\pi i}{M}\right) \quad \text{and} \quad s_{i1} = -E_s^{1/2} \sin\left(\frac{2\pi i}{M}\right). \tag{3.2.11b}$$

The ***Gram–Schmidt procedure***, whose flow chart is shown in Figure 3.2.4, is a systematic process for determining a minimal, but not unique, orthonormal basis set for any M-ary signal set. It begins by selecting the scaled version of $s_0(t)$ to be $\phi_0(t)$. Next $s_1(t)$ is projected onto this function, thus forming s_{10}, and the signal $s_{10}\phi_0(t)$ is removed

[7]Technically, the functions are orthonormal when $\omega_c = n2\pi/T_s$ or nearly so when $\omega_c \gg 2\pi/T_s$.

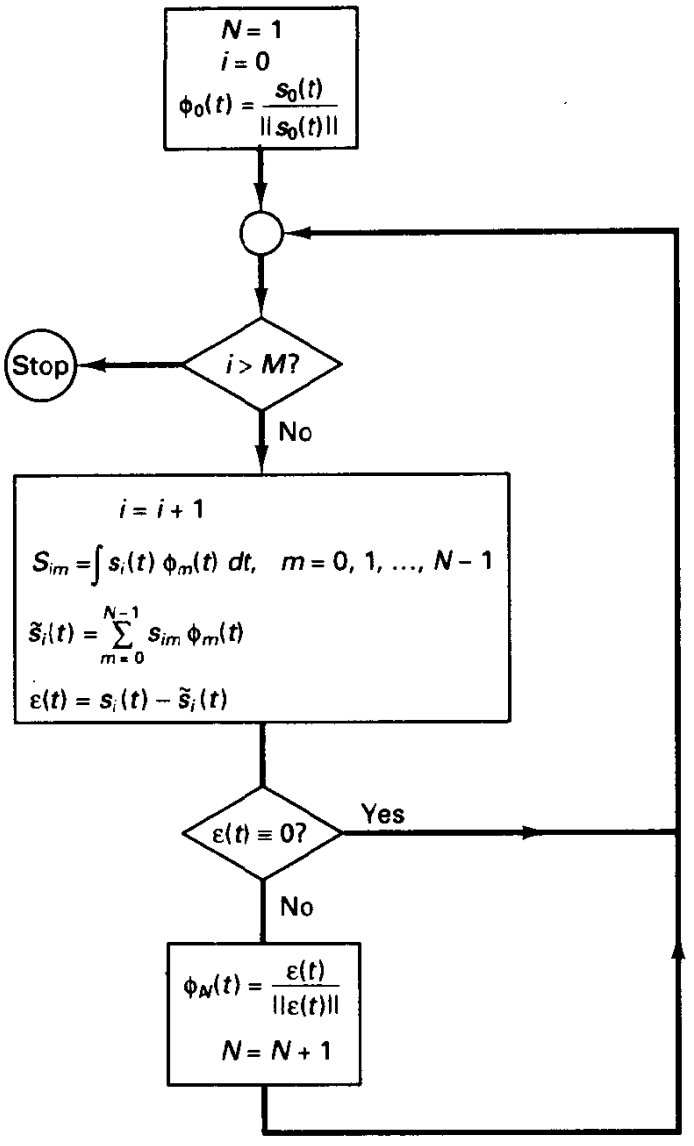

Figure 3.2.4 Gram–Schmidt flow chart, $\|s(t)\| = \left[\int s_i^2(t)\,dt\right]^{1/2}$.

from $s_1(t)$, the residual being orthogonal to the first basis function. A normalized version of this residual waveform becomes the second basis function, $\phi_1(t)$. The next signal is projected onto these two bases, the residual is found, and if nonzero, scaled to become the next basis function, and so on. The procedure repeats until the supply of signals is exhausted, possibly terminating with $N \leq M$. (Inequality occurs when the set of signals is linearly dependent; that is, one or more signals can be expressed as a linear combination of others.)

We now examine three important generic classes of signal sets and their signal constellations.

Example 3.1 General Antipodal Signals (Figure 3.2.5)

Two signals, irrespective of their detailed description, are ***antipodal*** if one signal is the negative of the other; that is, $s_1(t) = -s_0(t)$. Obviously, the signal constellation is $N = 1$

dimensional, with $\phi_0(t) = cs_0(t)$, the constant chosen to normalize the energy. The signal constellation appears as in Figure 3.2.5. Important examples are binary phase shift keying, binary NRZ (nonreturn to zero) signals, and sequence inversion modulation of spread-spectrum coded signals (see Exercise 3.3.2).

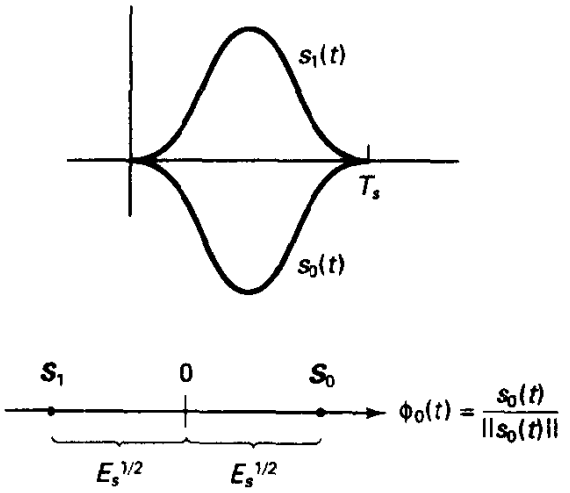

Figure 3.2.5 Antipodal signal example and signal constellation.

Example 3.2 General Orthogonal Signals (Figure 3.2.6)

We define an ***orthogonal*** signal set to consist of M equal-energy waveforms $s_i(t)$ with

$$\int_{T_i}^{T_f} s_i(t)s_j(t)\,dt = \begin{cases} E_s, & i = j, \\ 0, & i \neq j. \end{cases} \tag{3.2.12}$$

The signal constellation has dimensionality $N = M$, and by choosing $\phi_m(t)$ to be a scaled version of the mth signal, we have a constellation with a signal point located at distance $E_s^{1/2}$ from the origin along each coordinate axis, as pictured in Figure 3.2.6. Popular examples of orthogonal sets are the set of M nonoverlapping rectangular pulses (referred to as pulse-position modulation), M sinusoids of duration T_s displaced in frequency by $\frac{1}{2}T_s$ (M-ary

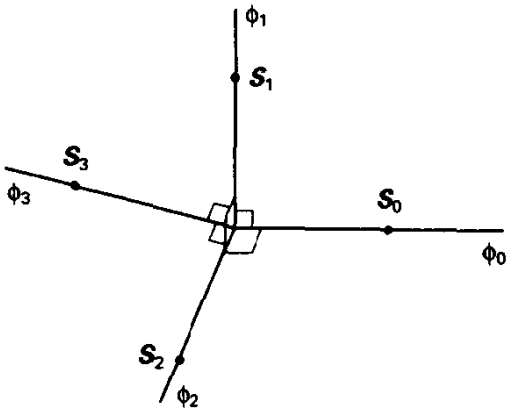

Four-dimensional
Cartesian Coordinates
(Schematically Illustrated)

Figure 3.2.6 Signal constellation for 4-ary orthogonal signals.

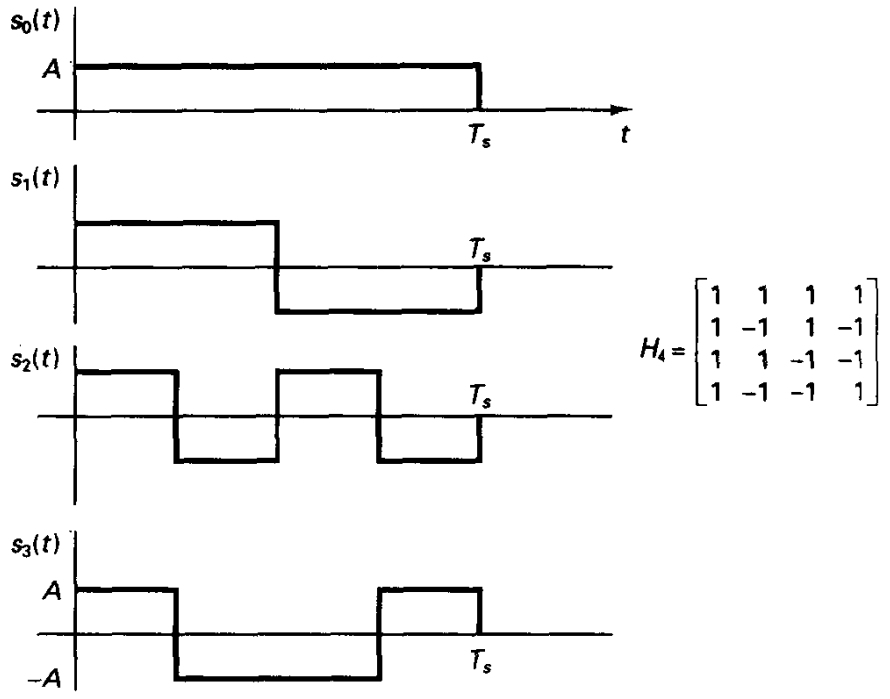

Figure 3.2.7 Four orthogonal signals derived from Hadamard (Walsh) matrix.

frequency shift keying), and binary sequences formed from rows of Hadamard matrices. A 4-ary Hadamard sequence construction in shown in Figure 3.2.7.

Example 3.3 Two-dimensional Constellations and QAM

A prevalent modulation technique exhibiting good spectral efficiency is formed by choosing

$$s_i(t) = a_i \left(\frac{2}{T_s}\right)^{1/2} \cos \omega_c t + b_i \left(\frac{2}{T_s}\right)^{1/2} \sin \omega_c t, \qquad 0 < t \leq T_s, \quad i = 0, 1, \ldots, M-1, \tag{3.2.13}$$

where the pairs (a_i, b_i) form the signal space coordinates in two dimensions. Typically, the pairs (a_i, b_i) are chosen from points on a two-dimensional square grid, or lattice. We can view the signal generation as amplitude modulation of phase-quadrature carriers, giving the name quadrature-amplitude modulation (QAM). Alternatively, we can regard (3.2.13) as amplitude and phase modulation of a single sinusoid (AM/PM). If all signals have equal energy, that is, $\left(a_i^2 + b_i^2\right)^{1/2} = E_s^{1/2}$, the modulation is strictly through the phase angle, and we refer to the signal set as M-PSK, with the constellation points located uniformly spaced on a circle with radius $E_s^{1/2}$.

A common variation, pulse-shaped QAM, uses a signal construction of the form

$$s_i(t) = h_T(t)\,[a_i \cos \omega_c t + b_i \sin \omega_c t], \qquad -\infty < t < \infty, \quad i = 0, 1, \ldots, M-1, \tag{3.2.14}$$

where $h_T(t)$ is a smooth transmitter pulse function extending beyond T_s seconds. The basis set is correspondingly modified by $h_T(t)$ but the two-dimensional signal constellation is unchanged.

3.3 SINGLE-SYMBOL DETECTION OF KNOWN SIGNALS IN AWGN

We now turn to the topic of optimal decision making and first consider a simple version of the general setting exhibited in Figure 3.1.1. We suppose that a ***single message symbol*** is conveyed by a single modulator signal and that the channel filter $H(f)$ has a nondistorting effect on the transmitted signal. Precisely, we assume that the channel medium has constant gain and a linear phase characteristic for all frequencies where the signals' Fourier transforms are nonzero. This implies that the received signal is a scaled, delayed replica of the transmitted signal; this delay introduces both symbol and carrier synchronization issues into the problem. The only additional channel effect is the addition of additive white Gaussian noise (AWGN). Our task is to make a minimum probability of error decision as to which signal was sent.

We will proceed to formulate the optimal receiver, or detector, for the case where the M signals are ***completely known*** at the receiver. By completely known signals, we mean that, in addition to knowing the functional form of all signals, which is naturally assumed, the receiver knows all relevant parameters about the *received* signals, especially the signal's arrival time, often referred to as having symbol timing available. In the case of bandpass, or carrier transmission, we assume in addition that the phase angle of the signal appearing at the demodulator input are perfectly known. Finally, should it be necessary, the various received signal amplitudes are known. These assumptions are tantamount to having perfect synchronization and gain measurement. The demodulator's determination of these parameters is certainly not a trivial task.

Although not the usual communication scenario, we justify the single-transmission/ideal channel assumption as follows. First, assumption of an ideal channel at the outset simplifies our development, meaning that, except for delay and amplitude, the received signals are the same as the modulator output signals. Once we have completed the description of the optimal processor for a single transmission on the ideal channel, it is straightforward to generalize to the distorting channel case, which we will do at the end of Section 3.3. Second, the single-transmission model avoids, for the present, complication of the decision making due to interaction at the receiver of signals produced by a sequence of message symbols. This phenomenon is broadly referred to as ***intersymbol interference*** (ISI). Such may occur either because the modulator signals extend in time beyond T_s seconds (and thus also the detector's processing interval for a given signal) or because the channel introduces memory in the form of $h(t)$, making signals formerly time limited to T_s seconds overlap into the adjacent signaling intervals at the receiver. This intersymbol interference phenomenon can have a devastating impact on system performance of a receiver designed in ignorance of its presence. In particular, decision errors may occur even in the absence of noise, and consequently its effect cannot be ignored on many channels. However, it may be shown that the first step in optimal detection of message sequences in an environment containing ISI and additive noise is to process the received signal exactly as if a single, isolated transmission were made through the distorted channel. This initial processing must be followed by a processor that "decodes" the memory induced by the channel. In summary, we claim that the case treated here is fundamentally important; the

signal processors developed here provide sufficient statistics for the more general setting.

Another need for emphasizing that we are treating a one-shot modulator transmission relates to coded transmission; that is, when the transmission has embedded redundancy, the optimal message decision is not formed by a sequence of M-ary symbol decisions as formulated here, followed by a decoder. Nonetheless, most of the basic steps in demodulation studied here are fundamental to optimal sequence decoding and in fact provide sufficient statistics for the sequence decision problem.

The problem then is the following: the modulator sends one of its M messages, denoted S_i, and conveyed in the form of a signal, $s_i(t)$, which is received by a fixed-amplitude, nondispersive channel. We define the ***average received energy per symbol*** to be E_s joules. Added to this waveform is white Gaussian noise having two-sided noise spectral density $N_0/2$ W/Hz. The receiver's observation interval is (T_i, T_f), which spans at least the time support of the signal. We wish to find the processor that minimizes the probability of decision error and ultimately to determine the resulting error probability.

Here's a sketch of the optimal receiver derivation. It relies on the Karhunen–Loeve [10] series expansion of the noise process, for which the (random) expansion coefficients are uncorrelated random variables. In general, this will require the adoption of special basis functions, called eigenfunctions, as discussed in Section 2.5, but for AWGN the eigenfunction selection is trivial. By this expansion, we are able to convert a decision problem involving a waveform observation into one involving a vector observation, a problem whose solution we have described in Chapter 2. The structure of this vector decision maker is then recast as a waveform processor.

We saw in the previous section that finite sets of deterministic signals may be viewed, by orthonormal series expansions, as points in N-dimensional space. Here we apply the same idea to the stochastic noise process. Consider an L-term series approximation, $N^{(L)}(t)$, for the noise process $N(t)$ over the observation interval (T_i, T_f):

$$N^{(L)}(t) = \sum_{m=0}^{L-1} N_m \phi_m(t), \tag{3.3.1}$$

where the basis functions $\{\phi_m(t)\}$ form an orthonormal set over the interval, and the expansion coefficients, now interpreted as random variables, are obtained by

$$N_m = \int_{T_i}^{T_f} N(t)\phi_m(t)\,dt, m = 0, 1, \ldots, L-1. \tag{3.3.2}$$

If the basis function set is complete, we may claim that, as L becomes large, $N^{(L)}(t)$ converges in mean-square to $N(t)$.[8] This is expressed as

$$\lim_{L\to\infty} E[(N(t) - N^{(L)}(t))^2] = 0. \tag{3.3.3}$$

The expansion coefficients are obtained by a linear operation, (3.3.2), on a Gaussian random process, and thus we know that the N_m are jointly Gaussian r.v.'s. By taking the expected value of both sides of (3.3.2) and then exchanging the order of expectation

[8]Technically, white noise does not satisfy the requirements for this convergence, because it is not a process with finite mean-square value. However, we may think of white noise as the limiting case of a process that is.

and integration, we find that the r.v.'s N_m have zero mean for all m. To establish the covariance of the noise coefficients, we form

$$\begin{aligned} E[N_m N_k] &= E\left[\int N(t)\phi_m(t)\,dt \int N(\tau)\phi_k(\tau)\,d\tau\right] \\ &= \int\int E[N(t)N(\tau)]\phi_m(t)\phi_k(\tau)\,dt\,d\tau \\ &= \int\int R_N(t-\tau)\phi_m(t)\phi_k(\tau)\,dt\,d\tau, \end{aligned} \tag{3.3.4}$$

which again follows from an interchange of orders of expectation and integration. By substituting the autocorrelation function of white noise, $R_N(\tau) = (N_0/2)\delta(\tau)$ in (3.3.4), and employing the shifting property of the Dirac impulse function to perform the integral, we obtain

$$E[N_m N_k] = \frac{N_0}{2}\int_{T_i}^{T_f} \phi_m(t)\phi_k(t)\,dt = \begin{cases} N_0/2, & m = k, \\ 0, & m \neq k. \end{cases} \tag{3.3.5}$$

Notice that (3.3.5) holds regardless of which orthonormal set we employ! Thus, for *any* orthonormal basis set, the noise expansion coefficients for white noise are uncorrelated, and since they are Gaussian, they are also independent. (More generally, to achieve this uncorrelatedness of the expansion coefficients, the basis functions must satisfy an integral equation involving the noise autocorrelation function [see Section 2.5] and the general solution is the Karhunen–Loeve expansion [10]).

We have thus determined that, for white Gaussian noise, projecting $N(t)$ onto a coordinate system defined by any orthonormal basis provides independent Gaussian random variables with zero mean and variance $N_0/2$. This projection operation is schematically illustrated in Figure 3.3.1, where the spherical symmetry of the p.d.f. for the L variables in an L-term expansion is indicated. Since any orthonormal basis set has these properties, the natural set to use incorporates the N-ary basis set employed to describe the signal set. We augment this set with additional orthonormal functions needed to complete the set. (It is actually immaterial how we complete the set since these additional expansion coefficients will be statistically independent of the signal index.)

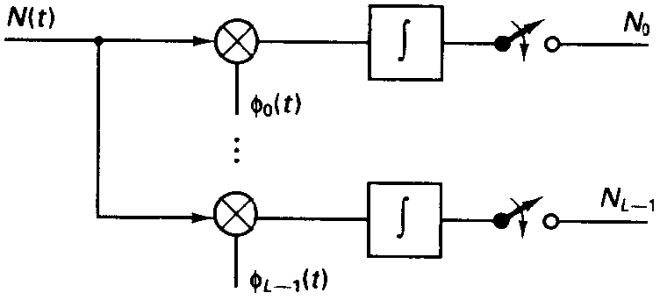

$$f(n_0, n_1, \ldots, n_{L-1}) = \frac{1}{(\pi N_0)^{L/2}} \exp\left[-(n_0^2 + \cdots + n_{L-1}^2)/N_0\right]$$

Figure 3.3.1 Obtaining noise coordinates from white Gaussian noise and resulting p.d.f.

Next we write a series expansion for the received signal $r(t) = s_i(t) + n(t)$, separating the contributions of the first N terms in the sum from the remainder:

$$r(t) = s_i(t) + n(t) = \sum_{m=0}^{N-1} r_m \phi_m(t) + \sum_{m=N}^{\infty} r_m \phi_m(t), \tag{3.3.6}$$

which recasts $r(t)$ in terms of an infinite-dimensional vector $(r_0, r_1, \ldots, r_{N-1}, \ldots)$. The first N components of this random vector, which we denote by $\mathbf{r}$, are given by

$$r_m = s_{im} + n_m, \qquad m = 0, 1, \ldots, N-1, \tag{3.3.7}$$

where the s_{im} are the signal-space coordinates. The remaining r_m are simply independent noise variables, n_m, are not statistically influenced by the choice of signal, and are clearly ***irrelevant*** to the detection problem. Thus, the relevant data are conveyed by the vector $\mathbf{r}$.

By this projection process, we have converted a waveform decision problem into a finite-dimensional vector decision problem, described in Chapter 2. There we found that the optimal policy to minimize error probability is the MAP rule:

$$\underset{i}{\text{maximize}}\ P_i f_{\mathbf{R}}(\mathbf{r}|S_i). \tag{3.3.8}$$

Because of the additive nature of the noise, we have $f_{\mathbf{R}}(\mathbf{r}|S_i) = f_{\mathbf{N}}(\mathbf{r} - \mathbf{s}_i)$, where $f_{\mathbf{N}}(\cdot)$ denotes the noise vector p.d.f. Coupling this with the fact that the noise coefficients are independent, zero-mean Gaussian r.v.'s, the MAP rule becomes

$$\underset{i}{\text{maximize}}\ P_i f_{\mathbf{N}}(\mathbf{r} - \mathbf{s}_i) \tag{3.3.9a}$$

or

$$\underset{i}{\text{maximize}} \left[P_i \prod_{m=0}^{N-1} \frac{1}{(2\pi\sigma^2)^{1/2}} e^{-(r_m - s_{im})^2/2\sigma^2} \right]. \tag{3.3.9b}$$

In maximizing a function over some decision set, it is permissible to maximize any monotone-increasing function of the original function. (The value of the maximized quantity will change under such transformation, but the optimizing parameter, here the decision index, will not.) Because of the product form and the exponential density functions in (3.3.9b), it is convenient to maximize instead the natural logarithm of the term in brackets in (3.3.9b). Doing so and recalling that $\sigma^2 = N_0/2$, we obtain the equivalent rule

$$\text{maximize} \left[\ln P_i - \frac{N}{2} \ln(\pi N_0) - \frac{1}{N_0} \sum_{m=0}^{N-1} (r_m - s_{im})^2 \right]. \tag{3.3.10}$$

By expanding the quadratic term and eliminating terms common to all i, we can just as well

$$\underset{i}{\text{maximize}} \left[\ln P_i + \frac{2}{N_0} \sum_{m=0}^{N-1} r_m s_{im} - \frac{1}{N_0} \sum_{m=0}^{N-1} s_{im}^2 \right]. \tag{3.3.11a}$$

The first term in (3.3.11a) accounts for prior probabilities, the second term is a scaled inner product between the received vector $\mathbf{r} = (r_0, r_1, \ldots, r_{N-1})$ and the signal vector $\mathbf{s}_i$, and the third term is the energy-to-noise density ratio for the ith signal. In vector notation, (3.3.11a) could be rewritten as

$$\underset{i}{\text{maximize}} \left[\ln P_i - \frac{E_i}{N_0} + \frac{2}{N_0} \mathbf{r} \cdot \mathbf{s}_i \right] \tag{3.3.11b}$$

The structure of a generic receiver shown in Figure 3.3.2, which we call a ***basis function receiver***, follows from (3.3.11). The receiver projects the received waveform into signal-space coordinates, computes vector inner products, and adds bias terms to account for the possibility of nonuniform prior probabilities and nonequal signal energies. Another interpretation can be given based on (3.3.10): project into signal space to obtain $\mathbf{r}$ and then decode to the closest signal in Euclidean distance (with possible addition of a bias for prior probabilities). In the case where the prior probabilities are equal and the signal energies are equal, the receiver biases can be dropped and we have the simplified receiver of Figure 3.3.3.

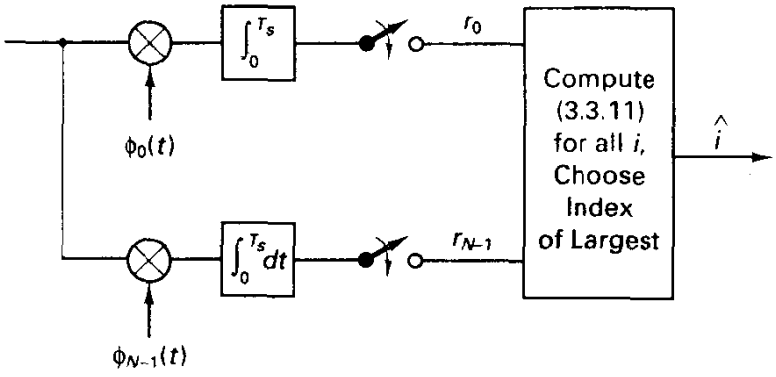

Figure 3.3.2 Optimal receiver for AWGN channel.

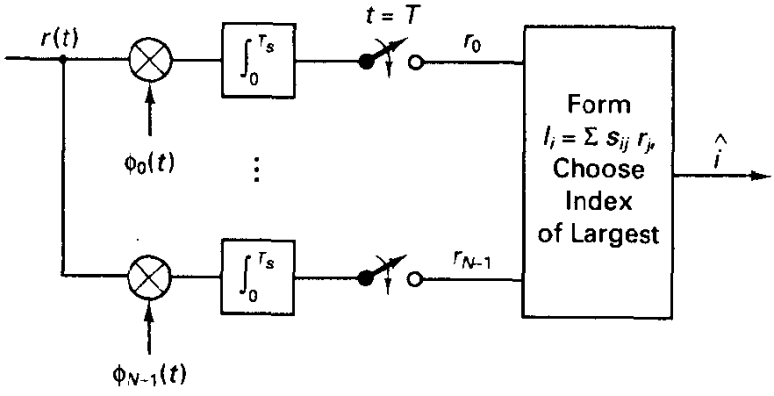

Figure 3.3.3 Optimal basis function receiver, equal priors, equal energies assumed.

An alternative receiver structure, referred to as a ***correlation receiver***, derives from realizing that the vector inner product in (3.3.11) could be extended in concept to arbitrarily large dimension, without changing the numerical result, by padding zeros in the higher-order positions of the signal vector. The vector inner product is precisely equivalent to the waveform correlation between waveforms of corresponding dimensionality (see Exercises 3.3.1 and 3.3.2), and in the limit as dimensionality increases we may write (3.3.11) as

$$\underset{i}{\text{maximize}} \left[\ln P_i + \frac{2}{N_0} \int_{T_i}^{T_f} r(t) s_i(t)\, dt - \frac{1}{N_0} \int_{T_i}^{T_f} s_i^2(t)\, dt \right]. \tag{3.3.12}$$

The second integral can be recognized as E_i and is a precomputed term. In this receiver the waveform projection is onto each of the M signals, instead of N basis functions, and biases again are included for prior probabilities and energies. This receiver is shown in Figure 3.3.4a for the general case and for the special case of equal priors and signal energies. (The scaling parameters such as $2/N_0$ in Figure 3.3.4 can be eliminated if other bias terms are properly modified; we include them since the scaling emerges naturally from the derivation.)

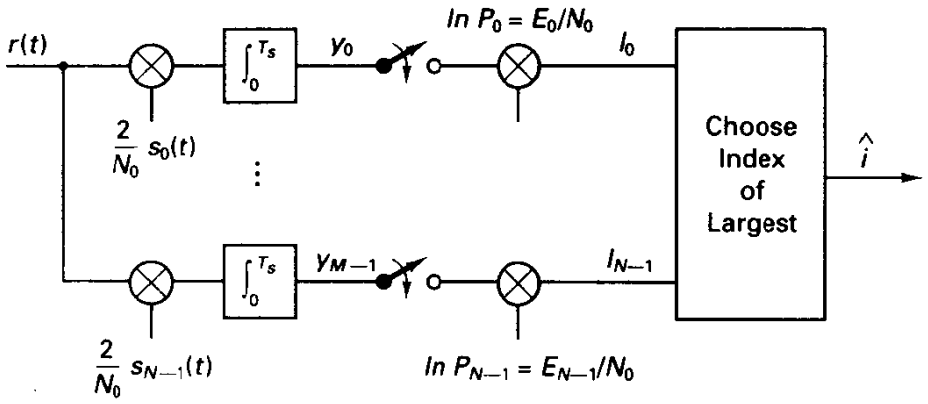

Figure 3.3.4a Optimal receiver in correlator form.

Despite the intuitively appealing correlation structure of the optimal processor, we caution that its derivation does hinge strongly on an AWGN assumption. Also, although we are at present interested in demodulation on a symbol-by-symbol basis, the derivation pertains equally well to situations where the signals are sequences of elementary signals, for example, codeword sequences. All we need to do to optimally detect such sequences, in principle, is to correlate with all *possible* signal waveforms, add any necessary bias terms, and choose the index of the maximum.

An equivalent version of the receiver of Figure 3.3.4b is known as the ***matched filter receiver*** and is obtained by noting that, in the ith channel of the correlation

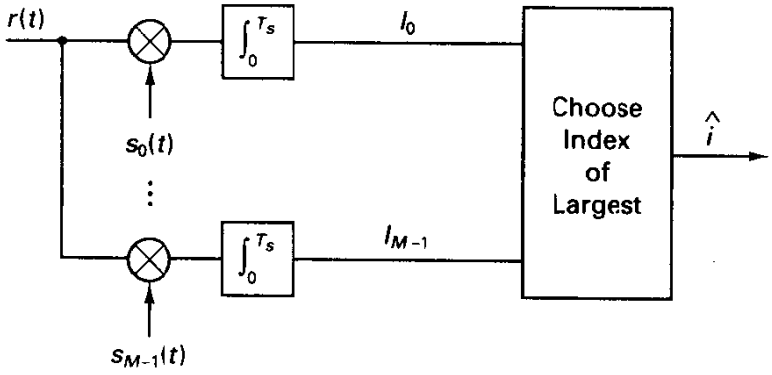

Figure 3.3.4b Correlation receiver for equal priors, equal energies.

receiver,

$$y_i = \int_{T_i}^{T_f} r(t)s_i(t)\,dt. \tag{3.3.13}$$

An identical way of generating y_i is with a linear filter $h_i(t)$ whose impulse response is

$$h_i(t) = s_i(T_f - t), \qquad T_i \le t \le T_f. \tag{3.3.14}$$

which may be verified by expressing the convolution of $r(t)$ with $h_i(t)$ and sampling the output at $t = T_f$. Thus, an optimal receiver is formed by a bank of filters whose impulse responses are the delayed, time-reversed versions of the signals.

It is instructive to interpret the matched filter in the frequency domain. The Fourier transform of the optimal filter impulse response is obtained by applying the time-scaling and time-shifting properties of the Fourier transform:

$$H_i(f) = S_i^*(f)e^{-j2\pi f T_f} = |S_i(f)|e^{-j[\arg S_i(f) + 2\pi f T_f]} \tag{3.3.15}$$

where $S_i(f)$ is the Fourier transform of the ith signal. Thus, the magnitude of the frequency response of the optimal filter follows that of the signal spectrum, which makes intuitive sense for a filter designed to "extract" signals from noise, but the phase response is just the negative of the signal's phase response (in addition to a linear phase term accounting for time delay). The latter makes the spectral components of the received signal properly "add up" at the sample time.

The matched filter is sometimes confused with the inverse filter, defined by

$$H_{\text{inv}_i}(f) = \frac{e^{-j2\pi f T_f}}{S_i(f)} = \frac{e^{-j[\arg S_i(f) - 2\pi f T_f]}}{|S_i(f)|} \tag{3.3.16}$$

The inverse filter also makes the spectral components of the signal add constructively at the sample time, but gives *low gain* to frequencies where the Fourier transform is large in magnitude. There is a big difference in terms of performance in noise.

The matched filter is often introduced in communication theory courses as the filter that maximizes the sample-time signal-to-noise ratio, defined as the ratio of the squared mean of the filter output at the sampling instant to the variance of the filter output. While being a reasonable optimization criterion, it does not directly address the minimum-error-probability objective. For Gaussian noise, these objectives coincide, but in a more general setting, maximizing this SNR is not necessarily optimal.

The parallel matched filter receiver is shown in Figure 3.3.5, *assuming equal priors and equal signal energies.* We remark that the correlation and matched filter receivers

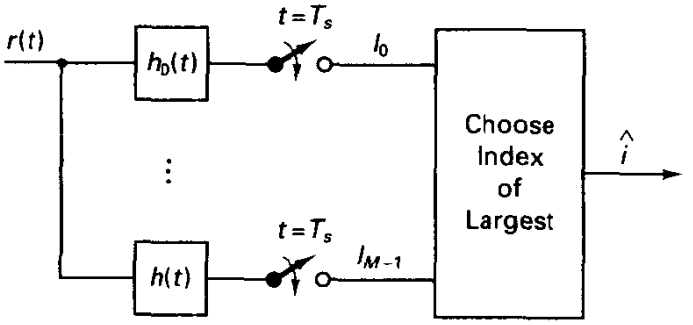

Figure 3.3.5 Matched filter version of optimal receiver.

are equivalent in that they form the same decision statistics l_i, but continuous-time waveforms found within the two processors, in particular just prior to the sampler, are quite different functions of time. It is also worth emphasizing at this point that the optimal receiver makes no attempt to avoid signal distortion, as an analog communication receiver might attempt. Instead, the task is merely deciding a signal index. This is one essential difference between the tasks of digital detection and estimation of analog waveforms.

We have now produced three distinct receiver structures, but all are equivalent in performance, for they produce the same decision. Preference for one of these receivers would be based on implementation issues. The matched filter realization may require synthesis of special filters, while the correlator version needs waveform generators and multipliers in general. In the case where the signal set dimensionality, N, is less than the number of signals, M, the implementation of Figure 3.3.3 is most appealing, because it minimizes the amount of waveform-level processing (signal generators, multipliers, integrators, and the like).

Whereas the receivers adopt a general time interval (T_i, T_f) that is at least as large as the signal durations, it is clear that, if the signal waveforms are identically zero outside some finite subinterval, then the various receivers will ignore $r(t)$ outside this latter interval, either through adoption of proper basis functions or through the time support of the waveform set in the correlation process. [The irrelevance of $r(t)$ outside the signal interval does not hold for nonwhite noise; see Exercise 3.3.3.] Many of the subsequent receiver structures will indicate processing over an interval of duration T_s, but this strictly is optimal only if the signal set is time-limited to this interval.

Example 3.4 Detection of Rectangular Polar Signals

We illustrate this discussion with perhaps the archetypal digital detection scenario, the optimal detection of rectangular,[9] polar signals in AWGN. The two signals, shown in Figure 3.3.6a, are assumed equiprobable and have equal energy, $E_s = A^2T$, defined at the input to the demodulator. Since the signals are constant over $[0, T_s]$, we may ignore the waveform multiplier shown in Figure 3.3.4a, in which case we obtain the receiver of Figure 3.3.6b. It is clear that an equivalent processor is that of Figure 3.3.6c, however, producing the unsurprising result that optimal decisions are made by integrating over one symbol and then comparing with zero. Again, this intuitively expected procedure is optimal only for the detection of polar rectangular pulses in AWGN. However, if the signals are rectangular and unipolar, we merely need to adjust the decision threshold.

This detector is sometimes known as the ***integrate-and-dump (I&D) detector*** since the integrator output is erased at the end of each bit before processing of the next. A typical active circuit realization is shown in Figure 3.3.7a. Still another realization that implements the matched filter structure and avoids the need for resetting the integrator is depicted in Figure 3.3.7b. In Figure 3.3.7c, we show the magnitude of the frequency response of the optimal filter, which has the same shape as the Fourier spectrum of the rectangular pulse by (3.3.15).

Figure 3.3.8 illustrates oscilloscope displays of the input and output of an integrate-and-dump detector. Observe that the unprocessed input signal appears rather prone to high error rate if a decision is based on a single sample of the input $r(t)$, but the optimal detector output is quite reliable.

[9]This signaling format is sometimes denoted as NRZ, for nonreturn to zero.

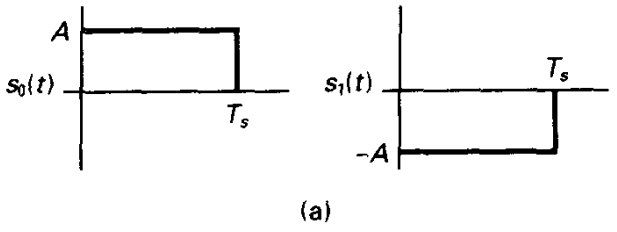

(a)

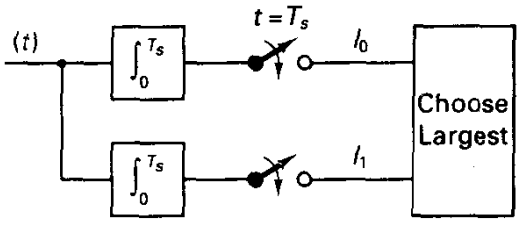

(b)

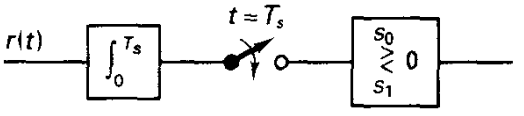

(c)

Figure 3.3.6 Development of optimal receiver for bipolar NRZ signals. (a) Antipodal signals (the NRZ example); (b) correlator receiver; (c) simplified correlator receiver.

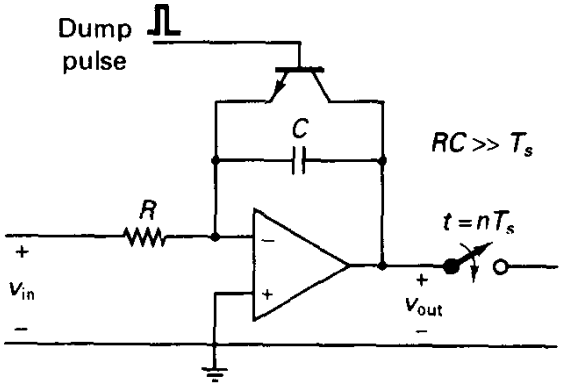

Figure 3.3.7a Op-amp realization of integrate-and-dump.

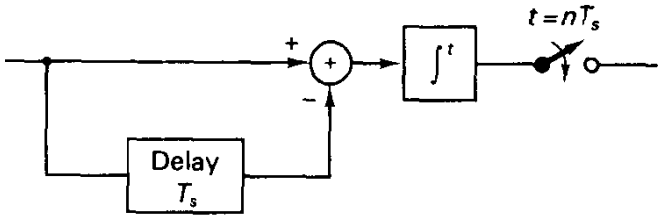

Figure 3.3.7b Another realization of matched filter for rectangular pulse.

From Figure 3.3.7c we note that the optimal detector is in some sense a low-pass filter, which is probably expected since the signal spectrum is low pass and the noise is wideband, but it is a filter we would not obtain by naive thinking about the problem. In particular, we might be led by intuition to process the received signal $r(t)$ with more traditional linear filters, such as a first-order low-pass filter, which has the desirable effect of noise removal.

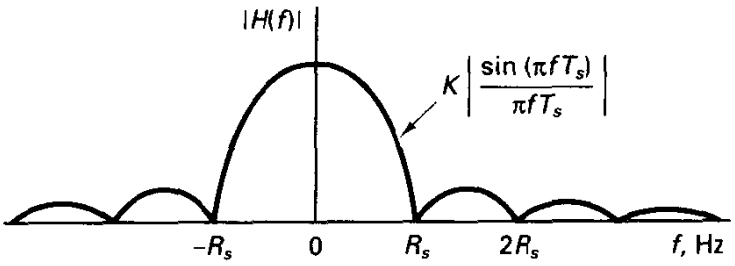

Figure 3.3.7c Magnitude of matched filter frequency response.

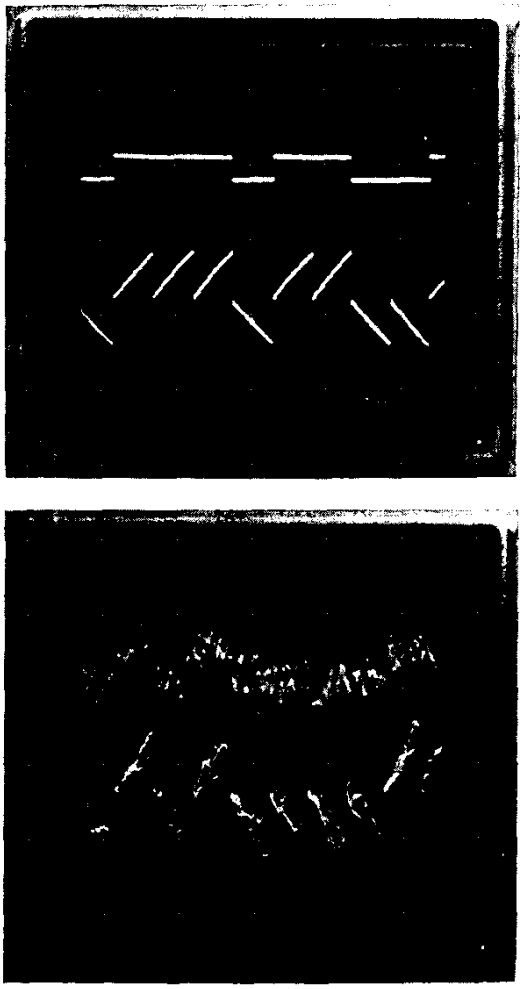

Figure 3.3.8 Oscilloscope photos for integrate and dump detection of NRZ signal; upper trace is $r(t)$, lower trace is I and D output prior to sampling. (top) Noiseless; (bottom) E_b/N_0 approximately 7 dB.

The reader is referred to Exercise 3.3.6 for a treatment of the trade-offs and deficiencies of this approach.

We have now formulated the general M-ary demodulator, and in the next several subsections, we specialize the structure in important practical cases as well as analyze the error performance.

3.3.1 Error Performance for General Binary Signals in AWGN

Especially compact results arise in the binary ($M = 2$) case, and, because binary signaling is prevalent in practice, we examine this case in detail.

The optimal receiver for two equiprobable signals is a two-channel correlator, the general form of which is shown in Figure 3.3.4. We may realize the same decision by use of the receiver of Figure 3.3.9, which correlates with the ***difference signal*** $s_0(t) - s_1(t)$. If the energies are not equal, we add a bias as indicated or, equivalently, adjust the decision threshold.

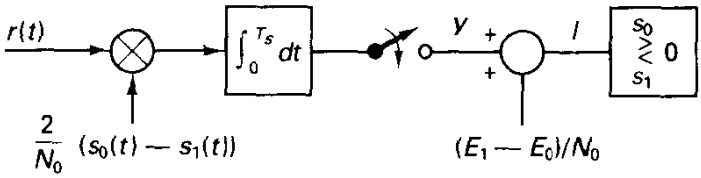

Figure 3.3.9 Optimal binary correlation receiver.

To analyze the performance in general, let us consider the mean of the random variable at the output of this correlator. Conditioned on transmission of $s_0(t)$, the mean, μ_0, of the variable Y is

$$\mu_0 = E[Y|s_0] = \frac{2}{N_0}\int s_0(t)[s_0(t) - s_1(t)]\,dt. \tag{3.3.17a}$$

Similarly, given transmission of $s_1(t)$, we have

$$\mu_1 = E[Y|s_1] = \frac{2}{N_0}\int s_1(t)[s_0(t) - s_1(t)]\,dt. \tag{3.3.17b}$$

The difference between the conditional means, defined as $\Delta\mu = \mu_0 - \mu_1$, is easily simplified to

$$\begin{aligned}\Delta\mu &= \frac{2}{N_0}\int [s_0(t) - s_1(t)]^2\,dt \\ &= \frac{2E_d}{N_0},\end{aligned} \tag{3.3.18}$$

where we have defined E_d as the ***energy in the difference signal*** $s_0(t) - s_1(t)$.

Furthermore, the variance of the decision variable is not dependent on which signal was transmitted and is easily shown to be

$$\begin{aligned}\sigma^2 &= \mathrm{Var}\left[\int [s_0(t) - s_1(t)]N(t)\,dt\right] \\ &= E_d\frac{N_0}{2},\end{aligned} \tag{3.3.19}$$

since the deterministic waveform we are projecting $N(t)$ onto is not a unit-energy basis function, but one that has energy E_d.

Figure 3.3.10 shows the two conditionally Gaussian distributions of the decision variable, along with an optimal threshold midway between the two means, chosen to

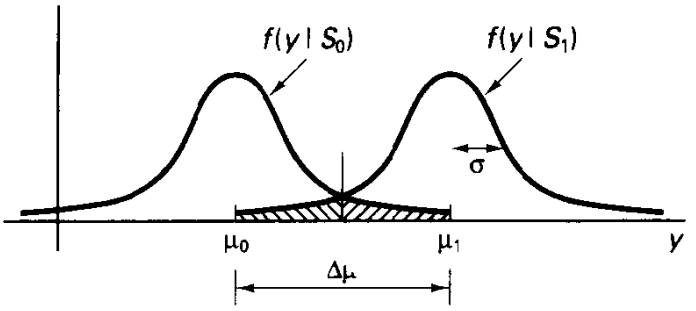

Figure 3.3.10 Conditional p.d.f.'s for general binary detection and error regions.

minimize the total error probability. The error probability is seen to be a Gaussian tail integral:

$$P(\epsilon) = P(\epsilon|s_0) \qquad \text{(by symmetry)}$$
$$= Q\left(\frac{\Delta\mu}{2\sigma}\right) = Q\left[\left(\frac{E_d}{2N_0}\right)^{1/2}\right], \tag{3.3.20}$$

illustrating the importance of maximizing the difference signal energy. This is intuitively a proper thing to do to enhance distinguishability, but is rigorously correct only for white Gaussian noise environments.

Another interpretation based on signal space ideas is provided by use of the basis function receiver. Recall that for $M = 2$ signals at most two basis functions are needed. Thus, we may place the two signals in two-dimensional space, arbitrarily chosen as shown in Figure 3.3.11. The received waveform is also projected to a point in the plane, and the optimal rule is "pick the closest signal." The perpendicular bisector divides the observation space into two half-space decision regions. Now, consider the transmission of signal $s_0(t)$. The received observation (r_1, r_2) will have a p.d.f. that is circularly symmetric about the point $\mathbf{s}_0 = (s_{00}, s_{01})$ (recall the fact that the noise coordinates are zero-mean, equal-variance independent Gaussian variates). The only component of the noise vector that is harmful to the decision process is that component in the direction *along the line connecting* $\mathbf{s}_0$ *and* $\mathbf{s}_1$. By symmetry, this random noise component is also

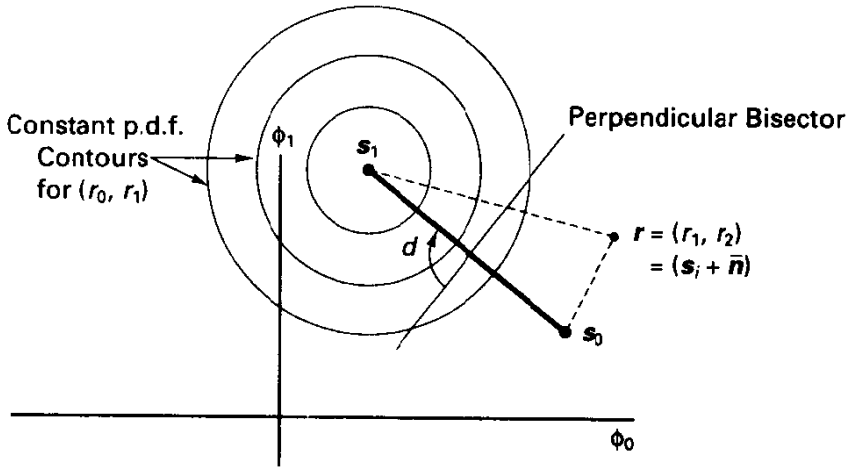

Figure 3.3.11 Signal-space geometry for general binary detection.

zero-mean with variance $N_0/2$. If this noise variable is more positive than $d/2$, where d is the intrasignal distance, an error occurs. Thus,

$$P(\epsilon|s_0) = \int_{d/2}^{\infty} \frac{1}{(2\pi N_0/2)^{1/2}} e^{-n^2/N_0}\, dn = Q\left[\frac{d}{(2N_0)^{1/2}}\right] \tag{3.3.21}$$

which follows after a change of variables in the integrand. It is clear that the same holds for $P(\epsilon|s_1)$, and thus the fundamental result is[10]

$$\boxed{P_s = P(\epsilon) = Q\left[\frac{d}{(2N_0)^{1/2}}\right] = Q\left[\left(\frac{d^2}{2N_0}\right)^{1/2}\right], \quad \text{general binary detection, AWGN.}} \tag{3.3.22}$$

This expression actually restates (3.3.20) since the energy residing in the difference signal is exactly the squared signal-space distance, as shown in (3.2.9).

It is a key point that only the squared signal-space distance between signals influences error probability, and performance is invariant to a translation or rotation of points in signal space. If we recall that in signal space the squared distance from the origin is the signal energy, the binary signal design problem now becomes quite clear: we wish to maximize the distance between signals, subject to an energy constraint, or a constraint on distance from the origin of signal space. The optimal signal design for $M = 2$ is the ***antipodal*** design; that is, $s_1(t) = -s_0(t)$, for which $E_0 = E_1 = E_s$ and $d = 2E_s^{1/2}$. For antipodal signals, *no matter what their detailed nature*, we have the important result that

$$\boxed{P_s = Q\left[\left(\frac{2E_s}{N_0}\right)^{1/2}\right], \quad \text{antipodal signaling, AWGN.}} \tag{3.3.23}$$

Several different antipodal designs are shown in Figure 3.3.12 with varying degrees of simplicity. We reemphasize that all sets have the same performance if properly detected, for a given E_s and N_0, although it is commonly misunderstood that wideband signals such as in Figure 3.3.12c require a greater signal-to-noise ratio for a given level of performance, since the receiver "admits more noise." (Actually, if we define signal-to-noise ratio as the ratio of total signal power to noise power measured in the signal bandwidth, a *smaller* SNR is allowed for wideband signals!)

While on the topic of SNR, we note that the figure of merit E_s/N_0 is

$$\frac{E_s}{N_0} = \frac{P_r T_s}{N_0} = \frac{P_r}{N_0 R_s} \tag{3.3.24}$$

The latter ratio could be interpreted as a signal power-to-noise power ratio, where noise power is defined in a bandwidth equivalent to that of the symbol rate, R_s. The experimental utility of such a definition is limited, however, by the fact that the actual signal bandwidth is often very different than the symbol rate.

Another prevalent signal design is the ***binary orthogonal*** design, whose signal constellation is shown in Figure 3.3.13, with some examples also indicated of actual

[10]Hereafter we will frequently use P_s to denote a symbol error probability.

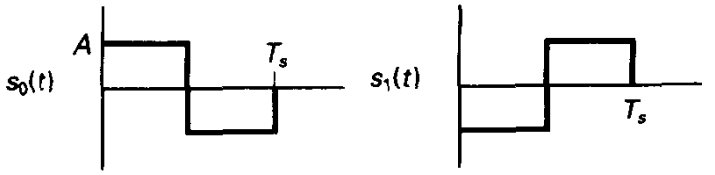

$$E_0 = A^2T_s = E_1;\ E_d = 4A^2T_s$$

(a)

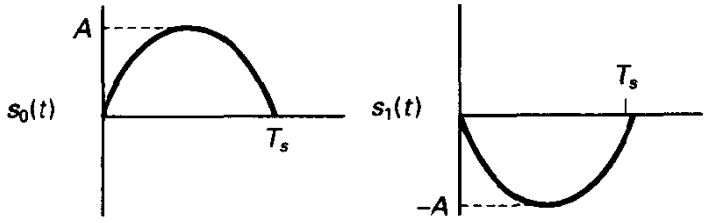

$$E_0 = E_1 = \frac{A^2T_s}{2};\ E_d = 2A^2T$$

(b)

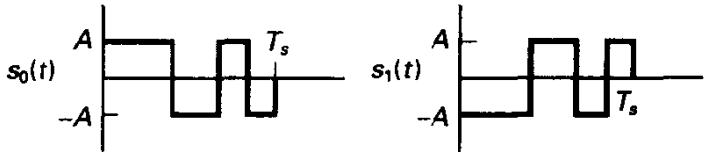

$$E_0 = E_1 = A^2T_s;\ E_d = 4A^2T_s$$

(c)

Figure 3.3.12 Examples of antipodal signals. (a) Manchester, or split-phase; (b) half-cycle sinusoid; (c) spread spectrum signals.

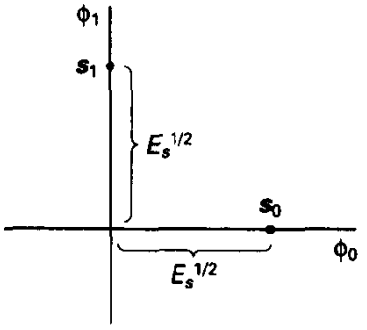

Figure 3.3.13 Constellation for binary orthogonal signals and example waveforms (a) pulse position modulation; (b) frequency shift keying.

waveforms for baseband and carrier signaling. Here, both signals have equal energy, but the signal-space distance between them is only $d = (2E_s)^{1/2}$, whence, from (3.3.22),

$$P_s = Q\left[\left(\frac{E_s}{N_0}\right)^{1/2}\right], \qquad \text{orthogonal signaling, AWGN.} \tag{3.3.25}$$

Finally, and of lesser interest, is ***on–off keying***, with a constellation shown in Figure 3.3.14. Here $E_1 = E_s$, $E_0 = 0$, $d = E_s^{1/2}$, and

$$P_s = Q\left[\left(\frac{E}{2N_0}\right)^{1/2}\right], \qquad \text{on–off signaling, AWGN.} \tag{3.3.26}$$

It is important to note the relative energy efficiencies of these three generic binary signal classes. Relative to antipodal signal sets, orthogonal sets require twice the energy-to-noise density ratio (or 3 dB more) for equal error probability, and on–off sets require four times (6 dB) greater E_s/N_0. To be fair to the on–off case, we should note that if a comparison is made on the basis of *average* energy consumption, rather than *peak* energy, then on–off is equivalent in energy utilization to orthogonal signaling and 3 dB inferior to antipodal. This follows since the average energy consumption in on–off keying is only half the peak energy.

Another subtle point about on–off keying is that the optimal decision threshold, or equivalently the bias term required in the receiver, depends on the received energy level, and some type of level control is essential if optimum performance is desired. (See Exercise 3.3.5.) Most commonly, this is provided by automatic gain control (AGC) in the receiver. Antipodal and orthogonal signals are not faced with this problem, since the signal energies are all equivalent, although AGC may be found in these demodulators for other engineering reasons.

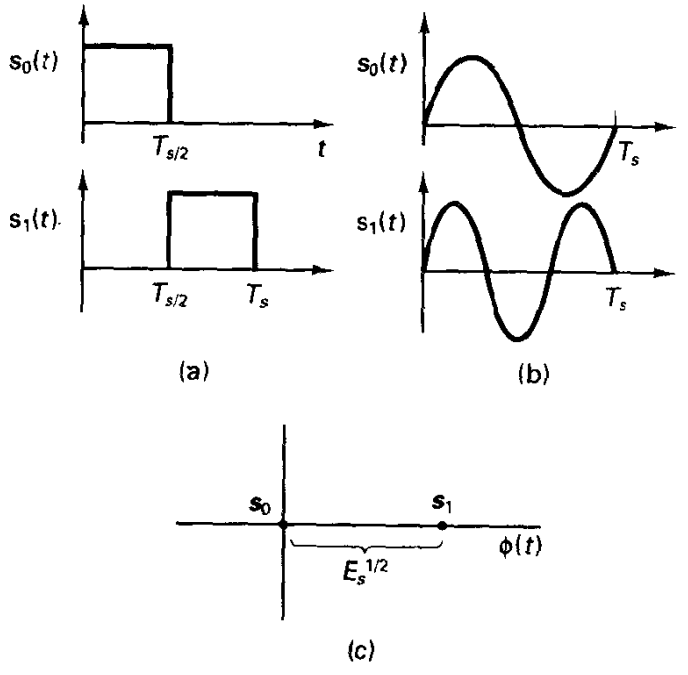

Figure 3.3.14 Constellation for binary on–off signaling.

3.3.2 Performance Bounds for *M*-ary Signaling

In the case of binary signaling, we were able to provide exact performance results for any signal set. In contrast, for nonbinary transmission either compact expressions are

not available for the exact performance, or numerical integration procedures must be invoked. In either situation, is is useful to accurately bound the true error probability as a function of energy-to-noise density ratio. This is surprisingly easy to do.

Two-signal Lower Bound

We recall that, under assumption of equal prior probabilities,

$$P_s = \frac{1}{M} \sum_{i=0}^{M-1} P(\epsilon|S_i). \tag{3.3.27}$$

Each term in the sum is lower bounded by the probability of confusing S_i (or $\mathbf{s}_i$) for its *nearest* signal-space neighbor. Denote this nearest-neighbor distance as $d_{\min_i}$. Then, by our expression for binary error probability in AWGN (3.3.22),

$$P_s \geq \frac{1}{M} \sum_{i=0}^{M-1} Q\left[\frac{d_{\min_i}}{(2N_0)^{1/2}}\right]. \tag{3.3.28a}$$

Because the minimum distances between constellation points are rather easily determined, (3.3.28a) provides a simple lower bound. Furthermore, if the signal set has symmetry so that all $d_{\min_i}$ equal some $d_{\min}$ (almost always the case in practice), then the lower bound simplifies to

$$P_s \geq Q\left[\frac{d_{\min}}{(2N_0)^{1/2}}\right]. \tag{3.3.28b}$$

Union Upper Bound

Consider transmission of the message S_0. An error occurs if the received vector $\mathbf{r}$ lies in the region of observation space $D_1 \cup D_2 \cdots \cup D_{M-1} = D_0^c$. This error region is the union of $M - 1$ half-spaces:

$$D_0^c = \bigcup_{j=1}^{M-1} D_{0j}' \tag{3.3.29}$$

where D_{0j}' is the decision region in favor of S_j when *only* S_j and S_0 are compared. In Figure 3.3.15, we show these half-spaces for the case of $M = 3$ signals in $N = 2$ dimensions.

We are interested in

$$P(\mathbf{r} \in D_0^c|S_0) = P\left(\bigcup_{j=1}^{M-1} D_{0j}'|S_0\right) \leq \sum_{j=1}^{M-1} P\left(D_{0j}'|S_0\right). \tag{3.3.30}$$

The last inequality follows from the union bound of Section 2.1, which gives name to the upper bound we are developing.

Each term in the sum of (3.3.30) is the probability of error in a *binary* decision problem. Thus,

$$P(\epsilon|S_0) \leq \sum_{j=1}^{M-1} Q\left[\frac{d_{0j}}{(2N_0)^{1/2}}\right], \tag{3.3.31}$$

where d_{0j} is the signal-space distance between $\mathbf{s}_0$ and $\mathbf{s}_j$. Arguing similarly for the other signals and letting the prior probabilities be equal, we have

$$P_s \leq \frac{1}{M} \sum_{i=0}^{M-1} \sum_{j \neq i} Q\left[\frac{d_{ij}}{(2N_0)^{1/2}}\right]. \tag{3.3.32}$$

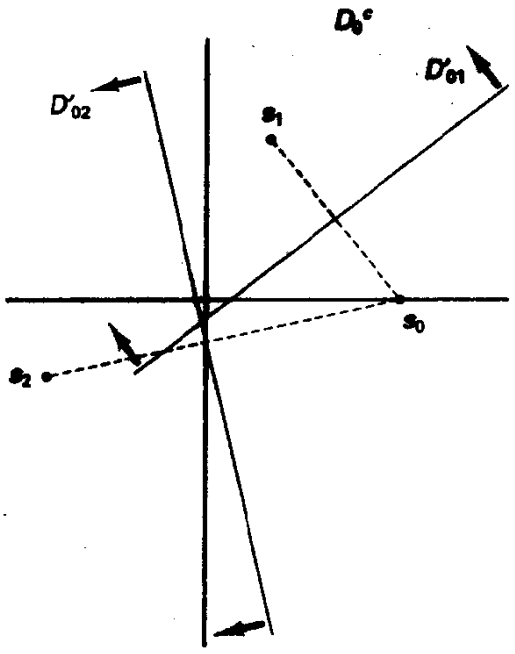

Figure 3.3.15 Error region D_0^c as union of error regions D_{0i} for binary choices.

For the ith signal, the inner sum is bounded by $M-1$ times the largest term of the sum, which in turn occurs when d_{ij} is *minimum* over j. Thus,

$$P_s \leq \frac{M-1}{M} \sum_{i=0}^{M-1} Q\left[\frac{d_{\min_i}}{(2N_0)^{1/2}}\right]. \tag{3.3.33}$$

A more compact, but slightly looser bound (unless all $d_{\min_i}$ are equal by symmetry), is the bound obtained by using the global minimum distance $d_{\min}$ in each term of the sum:

$$P(\epsilon) \leq (M-1)Q\left[\frac{d_{\min}}{(2N_0)^{1/2}}\right]. \tag{3.3.34}$$

Equation (3.3.34) is the principal result, requiring only the global minimum distance. Comparing it with (3.3.28), we see that the only difference is a multiplier $M-1$. While this is not a trivial difference for large M, we can say that the upper and lower bounds are exponentially equivalent,[11] despite the several stages of inequalities. This follows from exponential upper bounds for the Q-function derived in Chapter 2. Equivalently, at high signal-to-noise operating points, the additional energy needed to offset a factor of $M-1$ is increasingly negligible. Often, study of the decision zones will allow tightening of the multipliers still further, as in Example 3.8.

We illustrate the use of these bounds with a simple example.

[11]Two expressions for error probability, $P_1(x)$ and $P_2(x)$, are said to be exponentially equivalent if they exhibit identical exponential dependence on x, although differing by constants or algebraic factors dependent on x. The implication is that the difference in value of the exponent needed to achieve a given probability becomes vanishingly small as the target probability shrinks to zero.

Example 3.5 $M = 4$ Orthogonal Signals

A three signal orthogonal constellation is illustrated in Figure 3.3.16. Note that $d_{\min} = d_{ij} = (2E_s)^{1/2}$, and substitution into the bounds (3.3.28) and (3.3.34) produces

$$Q\left[\left(\frac{E_s}{N_0}\right)^{1/2}\right] \leq P_s \leq 3Q\left[\left(\frac{E_s}{N_0}\right)^{1/2}\right]. \tag{3.3.35}$$

As a measure of tightness of these bounds, we can compute the E_s/N_0 required to make the bounds equal 10^{-5}. Using a table of the Q-function and converting E_s/N_0 to decibels gives lower and upper bounds on E_s/N_0 of 12.55 and 13.0 dB, respectively. Clearly, the factor of 3 difference in the probability bounds does not manifest itself as a large difference in SNR requirements. Furthermore, the difference becomes smaller for lower P_s, depicting the exponential equivalence of the upper and lower bounds.

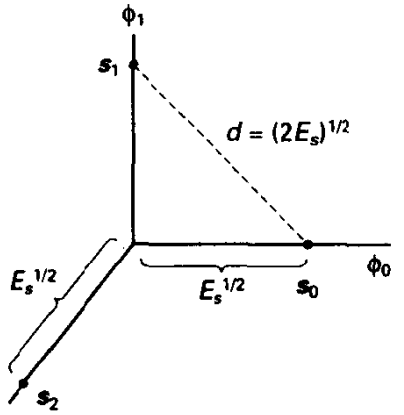

Figure 3.3.16 Signal constellation for $M = 3$ orthogonal signals.

3.3.3 Detection of M-ary Orthogonal, Biorthogonal, and Simplex Modulation

M-ary Orthogonal Case

Orthogonal signaling provides one means of achieving high energy efficiency in transmission (in fact, in the limit of large M it can achieve operation at channel capacity on the AWGN channel, as we shall see), but does so at enormous increase in complexity and bandwidth for large M. Examples of M-ary orthogonal signals are the following:

1. M-ary frequency shift keying, wherein one of M sinusoidal signals is selected every T_s seconds, with the tone spacing chosen to be some multiple of $\frac{1}{2}T_s$
2. M-ary pulse-position modulation (PPM), involving transmission of a pulse occupying one of M time slots within an interval T_s seconds
3. M-ary signaling using binary signal patterns formed by the rows of binary Hadamard matrices, these rows having mutual orthogonality (see Example 3.6)

We now proceed to evaluate the exact performance of such schemes as a function of E_s/N_0 on the AWGN channel. First, recall that the signal space is M-dimensional, with one signal located at distance $E_s^{1/2}$ from the origin along each coordinate axis. Each signal point of the constellation has $M - 1$ equidistant neighbors at Euclidean distance

$d = (2E_s)^{1/2}$. By symmetry, each signal has the same conditional error probability, $P(\epsilon|S_i)$, and this therefore equals $P(\epsilon)$. Thus, let's assume the transmission of $s_0(t)$, without loss of generality.

In the correlation receiver of Figure 3.3.4 the decision statistics are

$$y_i = \int \frac{2}{N_0} r(t) s_i(t)\, dt \tag{3.3.36}$$

and the decision is in favor of the largest correlation. Given our conditioning on the message S_0, the random variable Y_0 is distributed as

$$Y_0 \sim N\left(\frac{2E_s}{N_0}, \frac{2E_s}{N_0}\right), \tag{3.3.37}$$

while

$$Y_i \sim N\left(0, \frac{2E_s}{N_0}\right), \qquad i \neq 0. \tag{3.3.38}$$

[Again, our convention is that $N(\mu, \sigma^2)$ designates the Gaussian p.d.f. with mean μ and variance σ^2.]

The receiver errs if any $Y_i, i \neq 0$, exceeds Y_0. Thus, the probability of a *correct* decision is

$$P(C) = \int_{-\infty}^{\infty} P(\text{all } Y_1, Y_2, \ldots, Y_{M-1} < Y_0 | S_0) f(y_0|S_0)\, dy_0. \tag{3.3.39}$$

Because of independence of the r.v.'s Y_i, this expression may be written

$$P(C) = \int_{-\infty}^{\infty} \frac{e^{-(y_0-\mu)^2/2\sigma^2}}{(2\pi\sigma^2)^{1/2}} \left[\int_{-\infty}^{y_0} \frac{e^{-y^2/2\sigma^2}}{(2\pi\sigma^2)^{1/2}}\, dy\right]^{M-1} dy_0, \tag{3.3.40}$$

where $\mu = 2E_s/N_0$, and $\sigma^2 = 2E_s/N_0$. The inner integral is $1 - Q(y_0/\sigma)$, but this is as far as the expression can be reasonably simplified, and we must resort to numerical integration to evaluate the probability of symbol error $P_s = 1 - P(C)$. This numerical work was first reported by Viterbi [11] and is tabulated for $M = 2^m$ in Lindsey and Simon [12] as a function of bit energy-to-noise density ratio. We show the results for symbol error probability $P_s = 1 - P(C)$ in Figure 3.3.17.

The union bound is particularly easy to apply in this case since all signal pairs are equidistant in signal space. (This was applied in Example 3.5.) Recently, Hughes [13] has shown that a tighter bound on error probability for orthogonal signals is

$$P_s < 1 - \left\{1 - Q\left[\left(\frac{E_s}{N_0}\right)^{1/2}\right]\right\}^{M-1}$$

which in particular stays below 1 at low SNR.

It is often the case that we wish to compare options for modulation and detection, including cases with differing alphabet sizes M, all designed to support a certain *bit* rate with a common power constraint at the receiver, P_r watts. In such cases, it is important to compare the performance in terms of equal ***energy per bit received***, which is $E_b = P_r T_b = P_r T_s / \log_2 M = E_s / \log_2 M$, since each M-ary symbol conveys $\log_2 M$ bits in uncoded memoryless modulation. Thus, in presenting performance results, we

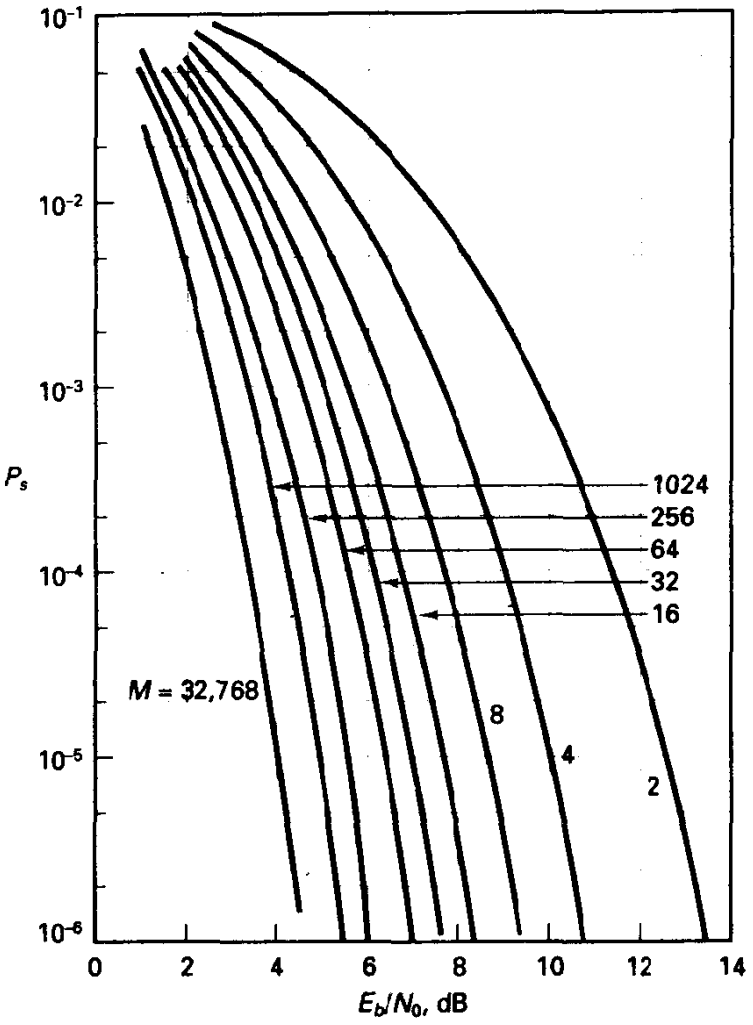

Figure 3.3.17 Symbol error probability for coherent detection of orthogonal signals.

should plot against E_b/N_0, using $E_s/N_0 = (E_b/N_0) \log_2 M$. Such a normalization has been done in Figure 3.3.17.

Warning: Authors do not always subscribe to the preceding suggestion, and it is easy to overlook the fact that schemes may be compared on different definitions of energy-to-noise ratios. Similarly, there is a choice whether to display symbol error probability or bit error probability, which is discussed below.

A signal-space inspection of the M-ary orthogonal constellation reveals that, to maintain a fixed symbol error probability, E_s must increase with M since the number of nearest neighbors increases. However, the efficiency measured in E_b/N_0 actually improves, at least for small error probability, as shown in Figure 3.3.17. We are led to ask